Isoform-specific C-terminal phosphorylation drives autoinhibition of Casein Kinase 1

Rachel Harold[1]*, Nikhil K. Tulsian[2,3]*, Rajesh Narasimamurthy[4], Noelle Yaitanes[1], Maria G. Ayala Hernandez[1], Hsiau-Wei Lee[1], David M. Virshup[,4,5]‡, Carrie L. Partch[1,6,7]‡,

[1]Department of Chemistry & Biochemistry, University of California Santa Cruz, Santa Cruz, CA 95064
[2]Department of Biochemistry, National University of Singapore, Singapore 117546
[3]Department of Biological Sciences, National University of Singapore, Singapore 117543
[4]Program in Cancer and Stem Cell Biology, Duke-NUS Medical School, Singapore, 169857
[5]Department of Pediatrics, Duke University Medical Center, Durham, NC 27710
[6]Center for Circadian Biology, University of California San Diego, La Jolla, CA 92093

[7]Lead contact
*Equal contributions
‡Correspondence: david.virshup@duke-nus.edu.sg, cpartch@ucsc.edu

Summary

Casein kinase 1 δ (CK1δ) controls essential biological processes, including circadian rhythms and Wnt signaling, but how its activity is regulated is not well understood. CK1δ is inhibited by autophosphorylation of its intrinsically disordered C-terminal tail. Two CK1 splice variants, δ1 and δ2, differ only in the last 16 residues of the tail and have different activity *in vivo*, suggesting that the extreme C-terminus (XCT) of CK1 plays a role in autoinhibition. Using NMR and HDX-MS, we show that the δ1 XCT is preferentially phosphorylated by the kinase and the δ1 tail makes more extensive interactions across the kinase domain. Mutation of δ1-specific XCT phosphorylation sites disrupts its interaction with the kinase domain and increases kinase activity *in vitro* and in cells. δ1 autoinhibition relies on conserved anion binding sites around the CK1 active site, demonstrating a common mode of product inhibition of CK1δ. These findings demonstrate how a phosphorylation cycle controls the activity of this essential kinase.

Introduction

Kinases play a crucial role in biology through their ability to post-translationally modify proteins by phosphorylation, altering the structure and/or activity of their targets. The activity of most kinases is therefore kept under tight regulation, requiring phosphorylation of their activation loops or binding to cofactors or scaffolds to remodel the active site and/or recruit substrates; in some cases, removal of inhibitory phosphorylation can activate kinases (Endicott et al., 2012; Huse & Kuriyan, 2002). The kinase domains of Casein Kinase 1δ (CK1δ) and its paralog, CK1ε, are constitutively active, but autophosphorylation of their intrinsically disordered C-terminal extensions, or 'tails', inhibits kinase activity (Cegielska et al., 1998; Graves & Roach, 1995). CK1δ/ε tails are also targeted by a number of other kinases (Eng et al., 2017; Knippschild et al., 2014) and phosphatases (Cegielska et al., 1998; Liu et al., 2002; Partch et al., 2006; Rivers et al., 1998) *in vivo,* suggesting a dynamic mode of kinase regulation that is not well understood. Given the involvement of CK1δ/ε in a wide range of pathways from Wnt signaling, cell division, and apoptosis to circadian rhythms (Knippschild et al., 2014), understanding how the kinase activity of CK1δ/ε is regulated by phosphorylation of their intrinsically disordered tails could shed light on underappreciated regulatory mechanisms.

In mammalian circadian rhythms, CK1δ/ε regulate the intrinsic timing of the molecular clock through phosphorylation of the Period (PER) proteins (Etchegaray et al., 2009; Lee et al., 2009; Narasimamurthy & Virshup, 2021). A phosphoswitch involving competing CK1δ/ε-dependent sites on PER2 regulates its half-life (Zhou et al., 2015), wherein phosphorylation of a β-TrCP degron and subsequent protein turnover are counteracted by phosphorylation of several serines located within the Casein Kinase 1

binding domain (CK1BD) that anchors the kinase to PER throughout its daily life cycle (An et al., 2022; Aryal et al., 2017; Cao et al., 2023). These stabilizing phosphorylation sites occur within the Familial Advanced Sleep Phase (FASP) region, named for a point mutation in human *Per2* (S662G) that eliminates the priming phosphorylation and shortens the clock by ~4 hours, causing an extreme advance in the onset of sleep (Toh et al., 2001; Xu et al., 2007). We recently showed that phosphorylation of the PER2 FASP region leads to feedback inhibition of the anchored kinase, utilizing two highly conserved anion binding sites on CK1δ near the active site that bind phosphoserines in the FASP to block access to substrates (Philpott et al., 2022). This is similar to feedback inhibition of the kinase observed in DNA damage-induced apoptosis (Gebel et al., 2020). Conservation of these feedback inhibition binding modes establishes the importance of CK1δ/ε anion binding sites for regulation of the kinase by phosphorylated substrates.

Alterations in CK1δ/ε can also shift the balance of the phosphoswitch to have a profound effect on circadian timing in mammals from rodents to humans. These alterations include inherited polymorphisms (Lowrey et al., 2000; Philpott et al., 2020; Ralph & Menaker, 1988; Xu et al., 2005) and alternative splicing of CK1δ (Fustin et al., 2018). The two CK1δ splice isoforms, δ1 and δ2, are identical throughout the kinase domain and most of the intrinsically disordered tail, differing only in the last 16 amino acids of the C-terminus (Fig. 1A), a region we call here the extreme C-terminus, or XCT. Despite this relatively minor change, the δ1 and δ2 isoforms differentially phosphorylate the PER2 FASP region *in vivo* to control circadian period (Fustin et al., 2018). Truncating the XCT at residue 400 is sufficient to derepress kinase activity (Narasimamurthy et al., 2018), suggesting a crucial role for residues 400-415 in regulation of CK1 activity in cells.

In this study, we examined the biochemical role of the XCT in differential regulation of CK1δ isoform activity. We found that isoform-specific differences in CK1 activity are intrinsic to the kinase *in vitro*; CK1δ1 is autoinhibited to a greater extent than CK1δ2, and truncation of the isoform-specific extreme C-termini essentially eliminates autoinhibition. NMR assays of the δ1 tail with the kinase domain in *trans* or *cis*, via segmental isotopic labeling, revealed that interaction between the kinase domain and δ1 tail is dependent on phosphorylation and predominantly localized to the δ1-dependent sequence. By contrast, the δ2 tail interacts with the kinase domain even in the absence of phosphorylation, consistent with inhibition data using isolated δ1 or δ2 peptides. Using hydrogen/deuterium exchange mass spectrometry (HDX-MS), we mapped how CK1 isoforms or mutants differentially protect the kinase domain and intrinsically disordered tails from deuterium exchange. Protection of the kinase active site in the presence of an inhibitory phosphoFASP peptide of PER2 (Philpott et al., 2022) mirrors protection by the two CK1δ isoforms, which is largely eliminated by deleting the XCT region with the Δ400 truncation or mutation of the δ1-specific serines to alanines. Our study defines isoform-specific mechanisms of CK1δ regulation and demonstrates a conserved mechanism of kinase inhibition by phosphorylated substrates.

Results

CK1δ isoforms δ1 and δ2 have different kinase activity *in vitro*

The alternatively spliced CK1δ isoforms, δ1 and δ2, differ only in the last 16 amino acids of the C-terminal tail (Fig. 1A). We previously showed that CK1δ1, CK1δ2, and a related isoform, CK1ε, can all catalyze the rate-limiting priming phosphorylation in the PER2 FASP region, with CK1δ2 and CK1ε demonstrating increased activity compared to CK1δ1 (Narasimamurthy et al., 2018). The kinase domains of CK1δ and CK1ε are highly conserved, and their intrinsically disordered C-terminal tails differ, although the XCT of CK1δ2 and CK1ε are quite similar (Fig. S1A). This suggested that the differences in activity we observed in cells might be due to their XCT; consistent with this, truncation of the last 16 amino acids of CK1δ1 (Δ400) eliminated its isoform-specific decrease in activity (Narasimamurthy et al., 2018).

To determine if isoform-specific differences in activity are intrinsic to the kinase, we established a pipeline to purify dephosphorylated full-length recombinant proteins (Fig. 1B). To demonstrate the effect of tail phosphorylation on CK1δ1, we first pre-treated full-length, dephosphorylated CK1δ1 with ATP to induce autophosphorylation and then measured its activity on the PER2 FASP priming site using an ELISA-based kinase assay. As expected, pretreatment of the kinase with ATP before the substrate was added significantly reduced FASP priming phosphorylation compared to untreated CK1δ1 (Fig. S1B). We then used *in vitro* kinase assays to measure the activity of the two CK1δ isoforms compared to the Δ400 truncation and the fully active, tail-less CK1δΔC kinase

domain. Activity was measured on a mutant of the human PER2 FASP region (S665A) that only allows for phosphorylation of the rate-limiting priming serine at S662 (Fig. 1C and S1C-D) (Philpott et al., 2022). Although differences in activity were modest, the activity of CK1δ1 on the PER2 FASP was significantly lower than CK1δ2 (Fig. 1D, E). Truncation of the XCT or the entire tail gave rise to activity that was similar to CK1δ2, recapitulating differences in the activity we observed in cells (Narasimamurthy et al., 2018) and suggesting that CK1δ1 has increased autoinhibition. We also quantified autophosphorylation in these assays. Relative to the full-length proteins, the isolated kinase domain showed minimal autophosphorylation, and the δ1 kinase was significantly less phosphorylated than δ2 or Δ400, despite having more serines and greater inhibition than either (Fig. S1E). These differences point to an important regulatory role for the CK1δ1 XCT.

Differences in regulation of the δ1 and δ2 tails by the kinase domain

Possible phosphorylation sites in the tail have been mapped on full-length CK1δ1 *in vitro* (Graves & Roach, 1995) and in cells, where a non-phosphorylatable (NP) mutant substituting all 28 serines and threonines in the tail to alanine eliminated its electrophoretic mobility shift and regulation by cellular protein phosphatases (Eng et al., 2017). However, these studies did not unambiguously identify phosphorylation sites nor regions required for autoinhibition. The δ1 tail is 125 amino acids long and predicted to be intrinsically disordered, and no part of it was captured in a crystal structure of the full-length kinase (Longenecker et al., 1998). Therefore, we turned to nuclear magnetic resonance (NMR) spectroscopy to monitor backbone chemical shifts on the ^{15}N δ1 tail alone or in the presence of equimolar amounts of the unlabeled kinase domain to better

understand potential regulatory mechanisms. The ^{15}N-^{1}H HSQC spectrum of the isolated ^{15}N δ1 tail exhibited limited chemical shift dispersion consistent with an intrinsically disordered protein, and addition of kinase domain in the absence of ATP resulted in very minor chemical shift perturbations (Fig. 2A, left), indicating that the tail and kinase domain did not interact in *trans* at these concentrations. However, incubation of the same sample with ATP for 2 hours at 25 ºC resulted in chemical shift perturbations in the ^{15}N δ1 tail backbone, as well as several new peaks downfield that correspond to phosphorylated residues (Fig. 2A, right), demonstrating that the kinase can phosphorylate its tail in *trans.*

Due to issues with peak overlap in the ^{15}N-^{1}H HSQC spectra, we turned to ^{13}C-direct detection experiments, using ^{15}N-^{13}C CON spectra that provide better resolution of the protein backbone in disordered proteins using the amide nitrogen and carboxyl carbon of the peptide bond (Bastidas et al., 2015). We assigned a majority of the peaks in the ^{15}N-^{13}C CON spectrum of the δ1 tail using ^{13}C-direct detection and standard NH-edited methods. Addition of unlabeled kinase to the ^{13}C,^{15}N δ1 tail in the absence of ATP showed minimal chemical shift perturbation in the tail, similar to our ^{15}N-^{1}H HSQC data (Fig. S2A). After ATP addition, we observed chemical shift perturbations at the same resonances as before (Fig. 2B), as well as some peak broadening. Shifts were localized primarily to the XCT of the δ1 tail, and to a lesser extent in a charged region from residues 305-320 that is predicted to have alpha-helical structure (Fig. 2C-E). By contrast, ^{15}N-^{1}H HSQC spectra of the isolated δ2 tail showed chemical shift perturbations upon addition of kinase domain alone (Fig. S2B, left) that were enhanced by the addition of ATP (Fig. S2B, right), suggesting that the δ2 tail may interact with the kinase domain in *trans* in a manner different from the δ1 tail. Peaks in the CON spectrum of the ^{13}C,^{15}N δ2 tail were

significantly broadened compared to the δ1 tail (Fig. S2C, D), limiting further NMR analyses of the δ2 tail. These data suggest that the XCT of CK1δ1 is a uniquely favored target for phosphorylation by the kinase, even in *trans*.

To determine how regulation of the δ1 tail is influenced when tethered to the kinase domain, we produced a segmentally isotopically labeled full-length kinase using an NMR invisible, natural abundance kinase domain attached to an ^{15}N-labeled δ1 tail through Sortase A-mediated ligation (Fig. S2E) (Kobashigawa et al., 2009; Theile et al., 2013). ^{15}N-^{1}H HSQC spectra of the isolated ^{15}N-labeled δ1 tail and the tethered tail appeared to be the same, aside from broadening of a single glycine (G296) near the ligation juncture (Fig. 2F), suggesting that the kinase domain and tail do not interact in the unphosphorylated state in *cis* as well. This helps explain why unphosphorylated full length kinase has similar initial activity to the isolated CK1 kinase domain. Addition of ATP to the tethered tail sample resulted in chemical shifts in the ^{15}N-labeled δ1 tethered tail backbone similar to those we observed in *trans* (compare Fig 2A and Fig. S2F), indicating that tethering did not substantially alter kinase domain interaction and phosphorylation of the tail, including activity on the XCT. To confirm this, we generated a minimal δ1 tail construct beginning at residue 376. We obtained chemical shift assignments for the phosphopeaks that correspond to the three phosphosites specific to the δ1 tail (Fig. 2G). Phosphorylation of these residues in the full-length CK1δ1 protein was confirmed by LC/MS-MS (Fig. S2G). Using ^{15}N-edited 1D ^{1}H spectra of the phosphoserine region (Fig. 2H), we were able to monitor the kinetics of phosphorylation of the δ1-specific residue S406. As expected, tethering increased the rate of phosphorylation compared to in *trans* (Fig. 2I) (Dyla & Kjaergaard, 2020). Collectively, our NMR studies revealed differences in

how the δ1 and δ2 tails interact with the kinase domain and demonstrated a preference for phosphorylation of the δ1-specific XCT serines by the kinase domain. The preferential phosphorylation of these XCT serines suggests they may play a critical role in the autoinhibition of CK1δ1.

To test if any of the XCT phosphorylation sites are indeed autophosphorylated in cells, we generated an antibody that specifically recognizes a phosphorylated serine in the sequence SVV (pSVV antibody) that corresponds to S411 of CK1δ1 (Fig. S2H, I). This pSVV antibody detected robust autophosphorylation of purified full-length CK1δ1, which correlated with the band shift of autophosphorylated CK1δ1 (Fig. 2J). We then assessed phosphorylation of the XCT region in cells expressing myc-tagged CK1δ1. Global phosphorylation of the CK1δ tail is regulated *in vivo* by an active cycle of autophosphorylation and dephosphorylation (Rivers et al., 1998). Consistent with this, accumulation of S411 phosphorylation was detected when cells were treated with calyculin A, a broad-spectrum inhibitor of cellular Ser/Thr phosphatases, revealing reversible phosphorylation of CK1δ1 S411 in cells (Fig 2K). This is also consistent with reports of CK1δ1 phosphorylation at residues S406, S407, and S411 from large-scale phosphoproteomics screens (Oppermann et al., 2009; Sacco et al., 2016). Phosphorylation of CK1δ1 S411 in cells was blocked by addition of the CK1δ/ε-specific inhibitor PF 670 (Fig 2L), indicating that it is due to autophosphorylation. These data establish that S411 in the XCT of CK1δ1 is autophosphorylated in cells in a reversible and dynamic manner, consistent with this being a potential regulatory phosphorylation site.

Structural dynamics of CK1δ by HDX-MS in the presence of nucleotides or inhibitors

Kinase domains interact with a number of ligands, from nucleotides and substrates to products and inhibitors, all of which can exert changes in dynamics or structure across the protein (Lorenzen & Pawson, 2014). To better understand autoinhibitory interactions between the kinase domain and tails of different CK1 isoforms, we turned to hydrogen-deuterium exchange mass spectrometry (HDX-MS) to characterize the conformational dynamics of different CK1δ isoforms. HDX-MS has been a powerful tool to provide insights into conformational dynamics in protein kinases (Konermann et al., 2011; Masson et al., 2019; Sheetz et al., 2022). We first explored the effects of nucleotide binding on the isolated kinase domain. Deuterium exchange measurements were carried out for CK1δΔC saturated with either ATP or its non-hydrolyzable analogue AMPPNP. Protection against deuterium incorporation upon binding to either nucleotide was predominantly observed across the N-terminal lobe and active site (Fig. 3A, Fig S3), with lower deuterium exchange in the bound state reflecting decreased solvent accessibility and increased H-bond formation between the nucleotide-interacting residues. At the active site, ATP binding led to stronger protection than AMPPNP binding, highlighting the specificity of their interactions with CK1δΔC (Fig. 3B). These effects are similar to those observed for other kinases including PKA, ERK2, IRK, and SRC, as reported by numerous studies (Hamuro et al., 2002; Hubbard, 1997; Lee et al., 2005; Shi et al., 2006). In addition to these direct 'orthosteric' effects, the binding of ATP and AMPPNP also elicited distal ('allosteric') conformational changes across the C-terminal lobe. Reduced deuterium exchange was observed across peptides spanning the DFG motif (residues

145-151), the activation loop (151-179), and loop L-EF (208-218), which are all centered around the substrate-binding cleft/groove (Fig 3A). No significant protection was detected in other regions of the C-lobe. Comparison of HDX-MS results also revealed the intrinsic dynamics of CK1δΔC, wherein peptides spanning the catalytic cleft and hinge region (residues 56-72) displayed bimodal isotopic distribution of mass spectra (Fig. 3C). The two populations indicate the open- and closed- conformations of CK1δΔC and the inherent inter-lobe interactions required for catalytic activity.

To validate HDX-MS as an approach to monitor inhibitory interactions on the kinase domain, we also looked at protection of CK1δΔC from deuterium exchange in the presence of a quadruple phosphorylated inhibitory peptide from the PER2 FASP region, known as the 4p-FASP. This interaction has been previously characterized by X-ray crystallography (Philpott et al., 2022). Comparing the HDX behavior between CK1δΔC in the absence and presence of 4p-FASP revealed a reduction in conformational flexibility throughout the kinase domain (Fig. 3D), with the largest effects observed at peptides covering the nucleotide-binding site (4-20), hinge region (56-72), activation loop (150-179), and substrate-binding cleft (residues 209-230) (Fig. 3E), close to two conserved anion binding sites (located around R178 and K224) that mediate a direct interaction with the 4p-FASP peptide (Philpott et al., 2022). Comparing the effects of 4p-FASP binding to the HDX profile of ATP-bound CK1δΔC (Fig. 3D, E), we found that a larger segment of the activation loop and C-lobe had reduced solvent accessibility with 4p-FASP. These HDX-MS results confirm and extend findings from the co-crystal structure and illustrate how a phosphorylated substrate interacts with the substrate binding domain to substantially impact the conformational flexibility of CK1δ.

HDX-MS reveals the impact of CK1δ isoforms on structural dynamics of the kinase

To explore how differences in isoform phosphorylation affect interactions within CK1δ, we preincubated CK1δΔC, CK1δΔ400, CK1δ1, and CK1δ2 for 15 min at 25 ºC with excess AMPPNP or ATP to block or promote autophosphorylation, respectively, and then compared deuterium exchange profiles by HDX-MS (Fig. 4). The HDX-MS results, shown as Woods differential plots, highlight the peptides that undergo significant protection from deuterium exchange in the presence of ATP in blue, while peptides with increased exchange are in red (Fig. 4A-D). Similar to the results shown in figure 3, we observed protection in CK1δΔC in peptides covering primarily the N-lobe and substrate-binding groove (Fig. 4A). Similar changes in HDX profiles were observed for CK1δΔ400, which lacks the XCT, including across the N-lobe at the hinge region and αC helix, and the activation loop in the C-lobe (Fig. 4B). Two peptides at the junction between the kinase domain and the tail (residues 293-312 and 304-320) experienced a small but significant increase in deuterium exchange, indicating increased flexibility of this region upon ATP binding, although no other significant changes were observed along the C-terminal tail of CK1δΔ400 (Fig. 4B).

The presence of CK1δ1 and CK1δ2 XCTs led to different degrees of protection comparing autophosphorylation conditions (ATP) versus the non-hydrolyzable analogue AMPPNP (Fig 4C, D). In the kinase domain, CK1δ2 differed from CK1δΔ400 by modestly enhancing protection of the nucleotide binding pocket (Fig 4D). However, CK1δ1, with its preferential phosphorylation sites in the XCT, was strikingly different. CK1δ1 autophosphorylation led to a large majority of peptides (71 peptides in CK1δ1 versus only 32 in CK1δ2) showing significant protection against deuterium exchange, spanning the

N-lobe and the C-lobe. Peptides spanning the length of the disordered tail on CK1δ1 also showed significant protection, suggesting solvent inaccessibility, possibly due to interdomain interactions. CK1δ2 also had many peptides in the C-terminal tail that showed protection against deuterium exchange, albeit to a lesser extent (Fig. 4D, E).

To further understand changes in structural dynamics mediated by phosphorylation, we analyzed residue-specific deuterium exchange by analysis of overlapping peptides, represented as heat maps for each construct (Fig. 4E). These provide a comparative overview of time-dependent changes in exchange kinetics across the protein, including the C-terminal tail, and how truncation or splice isoforms influence this. These changes likely reflect both orthosteric effects of nucleotide-binding, as well as allosteric effects induced by the nucleotide and phosphorylation of the C-terminal tail. Lower overall deuterium exchange across CK1δ2 suggests that the δ2 tail has different conformational dynamics and/or interactions with the kinase domain from the δ1 tail, consistent with our NMR data. Furthermore, the effect of different tail lengths on the conformational changes on the kinase domain are clear when monitoring the HDX profiles of CK1δ1 with its other isoforms. With shortening of tail from CK1δ1 to CK1δΔC, progressive decreases in deuterium exchange were observed across most peptides of the kinase domain (Fig. S4). The most notable changes were seen for peptides spanning the active site, anion binding sites, and substrate binding cleft. These results highlight the interactions mediated by the tail with the kinase domain to regulate autoinhibition.

Anion binding sites on the kinase domain play a role in autoinhibition by the δ1 tail

One defining feature of CK1 is two anion binding sites near the active site that participate in substrate positioning and the conformation of the activation loop

(Longenecker et al., 1998; Philpott et al., 2020). The phosphorylated PER2 pFASP peptide docks its phosphate groups into these sites that span the substrate binding cleft of the kinase, thus inhibiting kinase activity (Fig 5A, C) (Philpott et al., 2022). We sought to determine if the phosphorylated XCTs utilize these anion binding sites to inhibit the kinase in a similar manner. First, we tracked changes in deuterium exchange of different kinase constructs by HDX-MS in the presence and absence of ATP, looking specifically at several peptides that are proximal to anion binding site 1 (Fig. 5A, B) and site 2 (Fig. 5C, D). For anion binding site 1, CK1δ1 showed the greatest protection for all three peptides, with the 4pFASP-bound kinase, CK1δ2, and CK1δΔ400 showing moderate protection compared to CK1δΔC (Fig. 5B). For anion binding site 2, CK1δ1 and the 4pFASP-bound kinase showed greater protection than the others (Fig. 5D).

To determine if these sites play a role in inhibition by the tails, we looked at the effect of a single, well-characterized point mutation at each anion binding site (Philpott et al., 2020) on the ability of CK1δ1 or CK1δ2 to phosphorylate the PER2 FASP priming serine. Notably, these anion binding site mutations eliminated inhibition by the phosphorylated PER2 FASP region (Philpott et al., 2022). The K224D mutation impaired phosphorylation by CK1δ2 and CK1ΔC, which we attribute to impaired substrate positioning based on prior work (Philpott et al., 2020). Remarkably, the same mutant in CK1δ1 had no decrease in FASP priming (Fig. 5E, S5A-B). Likewise, disruption of site 2 (R127E) had a similar isoform-specific effect on autoinhibition (Fig. 5F, S5C-D), although the effect was more modest than for site 1. We propose that the impaired substrate positioning caused by mutation of the anion binding sites is counter-balanced by relief of autoinhibition in CK1δ1, perhaps due to reduced XCT binding at the mutated anion binding sites.

Isoform-specific sequences of CK1δ differentially inhibit the kinase domain

Prior studies have shown that at least two substrates phosphorylated by CK1, the PER2 FASP region and the phosphorylation activation domain (PAD) of p63, inhibit kinase activity by product inhibition (Gebel et al., 2020; Philpott et al., 2022). To test if this model holds for CK1δ tail autoinhibition, where the isoform-specific peptides encoded by the XCT can act as direct inhibitors of the kinase, we added variably phosphorylated δ1 or δ2 peptides to the kinase in *trans* (Fig. 6A). To look at their effect on kinase activity, we used ADP-Glo assays with two PER2 substrates, the FASP region and the Degron, measuring activity with excess phosphopeptide compared to a reaction without peptides. For both substrates, inhibition by the δ1 peptides relied more on phosphorylation of the XCT, and the phosphorylated δ1 peptides were generally more potent inhibitors than the δ2 peptides, although there were some differences in the efficacy for the two substrates (Fig. 6B, S6A).

We extended these findings to full-length CK1δ1 and tested if the δ1-specific phosphosites are necessary for inhibition in the full-length protein *in vitro*. We mutated the three unique phosphosites in δ1 to alanines (S3A: S406A/S407A/S411A) and compared the activity to wild-type CK1δ1 on the PER2 FASP S665A substrate (Fig. 6C, S6B). Consistent with the D1-A peptide data, the CK1δ1 S3A mutant showed a modest but significant increase in activity compared to CK1δ1 (Fig. 6C, D), demonstrating that phosphorylation of the extreme C-terminus is important for autoinhibition of CK1δ1.

We next tested if the S3A mutant altered the interaction and dynamics of the tail with the kinase domain as assessed by HDX-MS. Strikingly, we found a large decrease in protected peptides in CK1δ1 S3A relative to the wild-type enzyme ((from 71 to 19) Fig.

6E, S6C), spanning both the kinase domain and the C-terminal tail. Indeed, the protection of the kinase domain by CK1δ1 S3A most closely resembled the HDX-MS behavior for CK1δΔC (Fig 4A), suggesting a near-total loss of tail-kinase interaction in the mutant. Hence, phosphorylation of three serines in the CK1δ1 XCT is likely to be a prerequisite for the interaction of the C-terminal tail with the kinase domain.

These findings led us to examine how the CK1δ1 S3A mutation affected PER2 FASP phosphorylation and half-life in cells. FASP phosphorylation increases the stability of PER2 (Zhou et al., 2015). Expression of the more active, less autoinhibited forms of CK1δ, CK1δΔC (Fig. 1D), significantly increased the stability of PER2-Luc after cycloheximide treatment in HEK293 cells compared to CK1δ1 (Fig. 6F). CK1δ1 S3A behaved similarly to CK1δΔC, demonstrating that loss of XCT phosphorylation in δ1 relieved autoinhibition (Fig. 6F). As a further test of the effect of the S3A mutation, we measured kinase activity on the FASP priming site in cells. Deletion of the C-terminal tail of CK1δ1 (CK1δΔC) or its S3A mutation markedly increased FASP phosphorylation in full-length PER2 in cells (Fig. 6G, H). These results confirm that phosphorylation of the three CK1δ1-specific serines is important for its autoinhibition both *in vitro* and *in vivo*.

Discussion

CK1δ is considered a constitutively active kinase because it does not require phosphorylation of its activation loop to take on an active conformation. Instead, it relies on autophosphorylation of its C-terminal tail and/or feedback inhibition from phosphorylation of its substrates to regulate kinase activity (Cegielska et al., 1998; Graves & Roach, 1995; Philpott et al., 2022). While we are beginning to understand

mechanisms of feedback inhibition (Gebel et al., 2020; Philpott et al., 2022), the extent of intrinsic disorder and phosphorylation throughout the tail have impeded mechanistic understanding of autoinhibition. Since the CK1δ tail can be phosphorylated by other kinases to regulate its activity in cells (Bischof et al., 2013; Eng et al., 2017; Giamas et al., 2007; Um et al., 2007), the role of autophosphorylation *per se* in the regulation of kinase activity *in vivo* has been unclear. The kinase domain was recently reported to autophosphorylate a conserved threonine near the active site to modestly inhibit its activity and alter substrate selectivity (Cullati et al., 2022). We observed minimal autophosphorylation of the isolated kinase domain relative to the full-length isoforms, but further studies could look at the integration of regulatory autophosphorylation throughout the kinase. Critically, changes in circadian rhythms with two isoforms of CK1δ that differ only in the tail demonstrate unambiguously that the tails have an important role *in vivo* (Fustin et al., 2018; Narasimamurthy et al., 2018). However, it was not clear from these studies if isoform-specific differences in activity occurred due to regulation of the tail by other kinases or if they were intrinsic to CK1δ. Here, we show that CK1δ isoforms have inherent differences in activity arising from interactions of the kinase domain and its disordered tail that are specified by isoform-specific differences in autophosphorylation of the XCT.

NMR spectroscopy allowed us to track site-specific autophosphorylation of the CK1δ disordered tails for the first time. We found that the 3 serines of the δ1-specific XCT are preferentially phosphorylated over other sites in the tail, whether the tail is phosphorylated by the kinase in *trans* or covalently linked to the kinase domain in *cis*. Chemical shift perturbations provided strong evidence for phosphorylation-independent

effects of the kinase domain on the δ2 tail, although further analysis of the δ2 tail by NMR was limited due to extensive peak broadening in the absence of the kinase domain. This behavior is consistent with potential “fuzzy” intramolecular interactions within the δ2 tail, where the tail exhibits multiple transient conformations, as has been shown with other intrinsically disordered proteins (Arbesu et al., 2018; Wang & Wang, 2019). Isoform-specific differences in the dynamics of the disordered tails could contribute to decreased inhibition by the CK1δ2 isoform. Due to the sequence similarity of the XCT between CK1δ2 and CK1ε, the differences in tail dynamics we observed here could extend to CK1ε. The presence of disordered C-terminal tails in orthologs of CK1δ in other species also suggest that this could be a conserved mechanism of autoinhibition.

We recently showed that the phosphorylated PER2 FASP substrate inhibits CK1δ through interaction with its conserved anion binding sites flanking the substrate binding cleft to regulate circadian rhythms (Philpott et al., 2022). HDX-MS analysis of the kinase domain bound to the inhibitory 4p-FASP phosphopeptide showed increased protection from deuterium exchange near these sites, confirming that HDX-MS could map inhibitory interactions on the kinase domain. Of the two CK1δ isoforms, CK1δ1 showed the greatest deuterium protection across the kinase domain, similar to protection seen with the 4p-FASP peptide. Protection in the kinase domain was moderately reduced in CK1δ2 and essentially eliminated by truncation of the XCT or the S3A mutant that eliminated phosphosites unique to δ1, indicating that phosphorylation of the XCT plays a crucial role in autoinhibition by CK1δ1. We also observed significant protection of the intrinsically disordered tail upon autophosphorylation of both CK1δ1 and CK1δ2 that was eliminated with truncation of the isoform-specific sequences. This suggests that both tails make

extensive contact with the kinase domain, although we don't yet understand the specific details of these interactions. A previous study using crosslinking mass spectrometry proposed a possible contact site for part of the CK1ε tail on the kinase domain, although there were few crosslinks (Dahlberg et al., 2009), suggesting that further optimization is needed. Our HDX-MS data support a model where the tails make extensive contacts with the kinase domain, but neither the binding sites nor the orientation of the tail is clear yet.

Based on these results, we propose that autophosphorylation of the CK1δ tail dynamically changes its interaction with the kinase domain to regulate kinase activity. Here, we examined the effect of CK1δ autophosphorylation on the PER2 phosphoswitch, which controls PER2 stability and the period of circadian rhythms in mammals, including humans (Narasimamurthy & Virshup, 2021; Zhou et al., 2015). Recent reports identified a role for CRY-PER-CK1δ complexes in phosphorylating the CLOCK subunit of the core circadian transcription factor CLOCK:BMAL1 to suppress its transcriptional activation of target genes by displacing the complex from DNA (Aryal et al., 2017; Cao et al., 2021). Therefore, regulation of CK1δ activity by its isoform-specific tails could have several roles in regulating circadian rhythmicity, not only through modulating the stability of PER2 but also by instigating transcriptional repression through promoting the release of CLOCK:BMAL1 from DNA. CK1 isoforms also have major roles in pathways beyond circadian rhythms, such as apoptotic signaling (Brockschmidt et al., 2008; Knippschild et al., 2005), Wnt signaling (Cruciat, 2014; Del Valle-Perez et al., 2011; Gao et al., 2002), and it is overexpressed in several cancers (Rosenberg et al., 2015; Schittek & Sinnberg, 2014). Therefore, understanding its regulatory mechanisms goes beyond building a

mechanistic understanding of circadian rhythms and could help lead to the development of targeted inhibitors that regulate autoinhibition.

Acknowledgements

Funding for this work was provided by the US National Institutes of Health grants R01 GM107069 and R35 GM141849 (to C.L.P.), and Singapore Ministry of Health grant MOH-000600 to D.M.V.

Author contributions

Conceptualization: R.H., N.K.T., R.N., C.L.P., and D.M.V.; Investigation: R.H., N.K.T., R.N., N.Y., M.A.H., and H.-W.L.; Formal analysis: R.H., N.K.T., R.N., N.Y., and H.-W.L.; Writing – Original draft: R.H., N.K.T., R.N., and C.L.P.; Writing – Review & Editing: R.H., N.K.T., R.N., C.L.P., and D.M.V.; Supervision: C.L.P. and D.M.V.; Funding Acquisition: C.L.P. and D.M.V.

Declaration of interests

The authors declare no competing interests.

Figures and legends

Fig 1

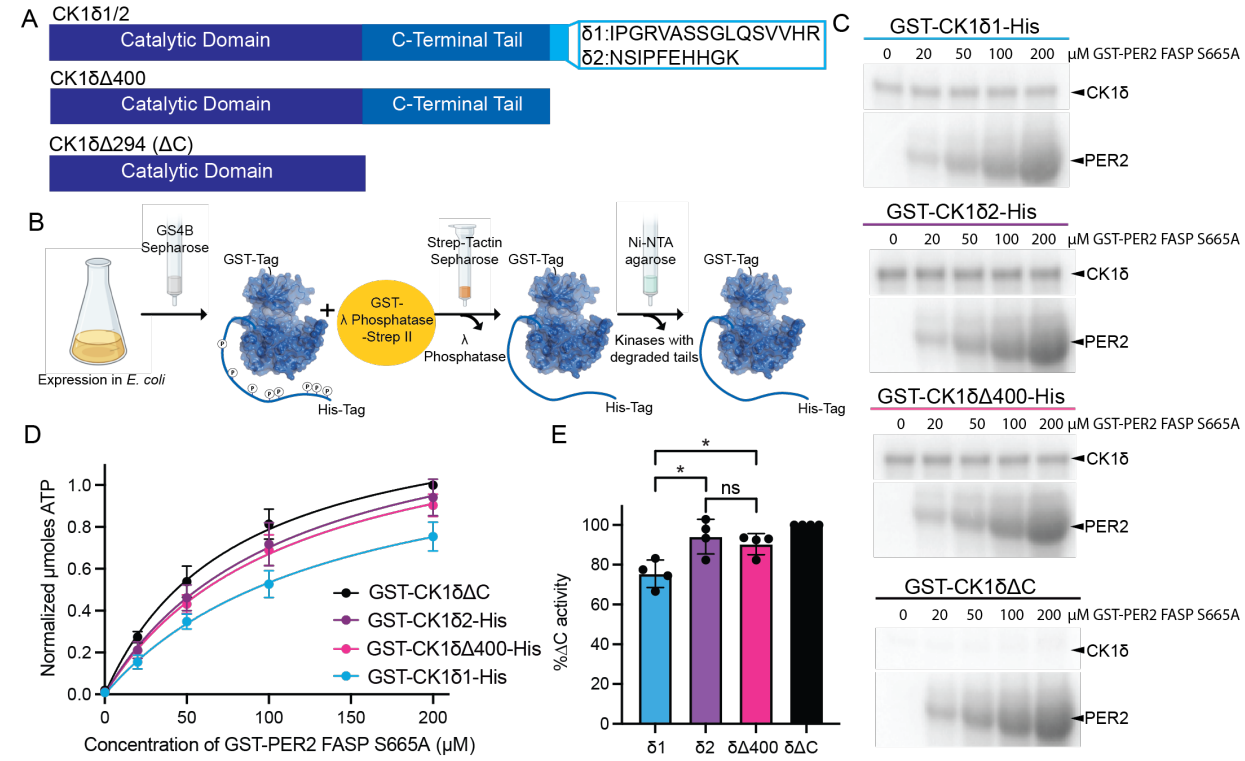

Figure 1 CK1δ isoforms alter kinase activity *in vitro*

A, Schematic of CK1δ isoforms and truncations. **B**, Kinase purification scheme with double tag system. **C**, Autoradiograph of ^{32}P kinase assay; top, autophosphorylation of kinase; bottom, priming phosphorylation of the PER2 FASP substrate. Representative autoradiograph from n = 4. **D**, Quantification of priming phosphorylation by CK1δ1 (blue), CK1δ2 (purple), CK1δΔ400 (pink), or CK1δΔC (black), normalized to CK1δΔC. **E**, Quantification of panel D. Ordinary one-way ANOVA, *, $p<0.05$ (n=4, mean ± s.d.).

Fig 2

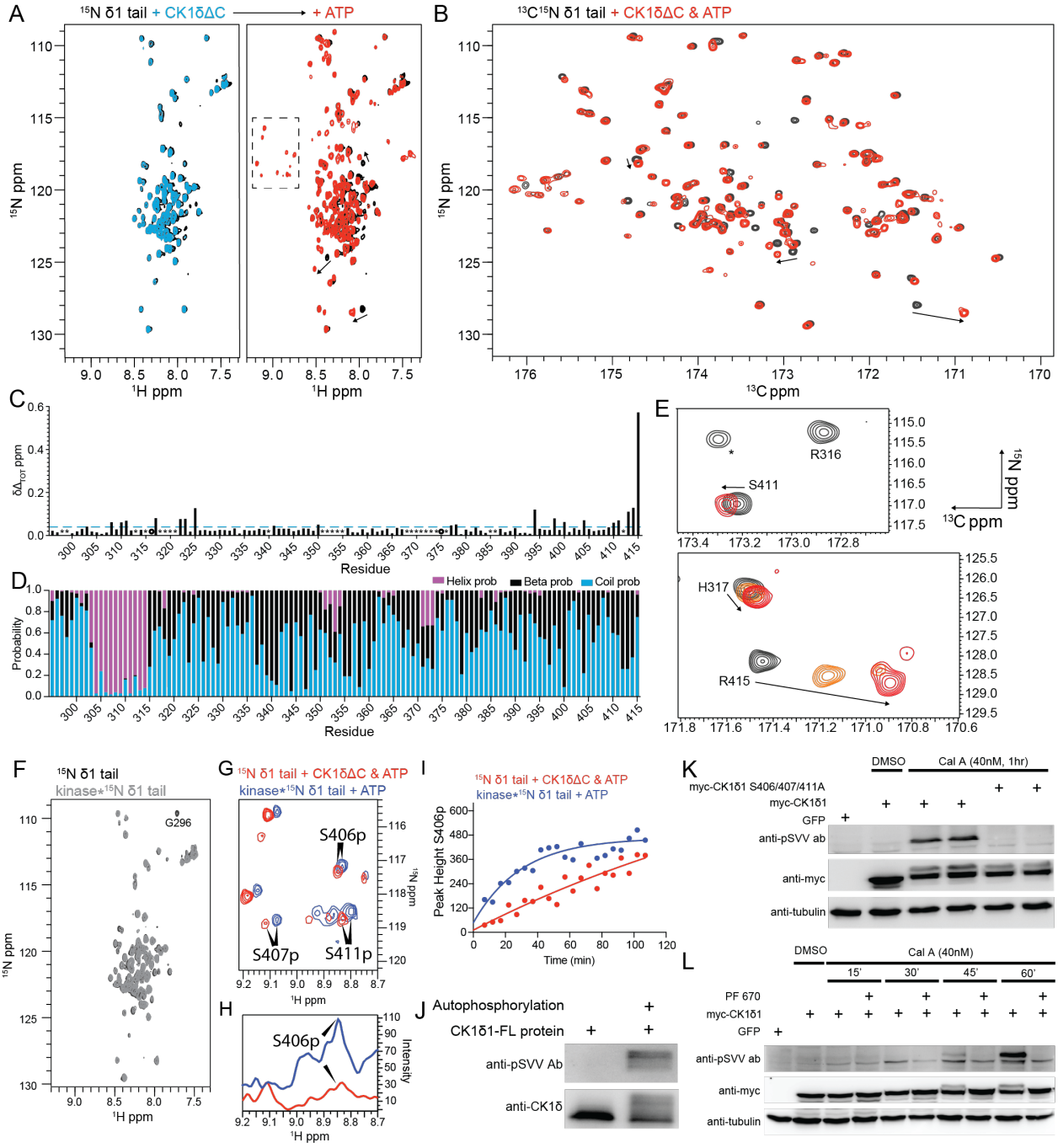
A
15N δ1 tail + CK1δΔC
+ ATP
15N ppm
1H ppm
B
13C15N δ1 tail + CK1δΔC & ATP
13C ppm
C
δΔTOT ppm
Residue
D
Helix prob
Beta prob
Coil prob
Probability
Residue
E
R316
S411
H317
R415
15N ppm
13C ppm
F
15N δ1 tail
kinase*15N δ1 tail
G296
G
15N δ1 tail + CK1δΔC & ATP
kinase*15N δ1 tail + ATP
S406p
S407p
S411p
H
S406p
Intensity
I
15N δ1 tail + CK1δΔC & ATP
kinase*15N δ1 tail + ATP
Peak Height S406p
Time (min)
J
Autophosphorylation
CK1δ1-FL protein
anti-pSVV Ab
anti-CK1δ
K
DMSO
Cal A (40nM, 1hr)
myc-CK1δ1 S406/407/411A
myc-CK1δ1
GFP
anti-pSVV ab
anti-myc
anti-tubulin
L
DMSO
Cal A (40nM)
15'
30'
45'
60'
PF 670
myc-CK1δ1
GFP
anti-pSVV ab
anti-myc
anti-tubulin

Figure 2 Phosphorylation-dependent interaction of the δ1 tail with the kinase domain

A, ^{15}N-^{1}H HSQC spectra of 100 μM ^{15}N δ1 tail alone (black) or in the presence of 100 μM CK1δΔC (blue), or 100 μM CK1δΔC and 2.5 mM ATP for 2 hours at 25 ºC (red); dashed box, peaks corresponding to phosphorylated residues. Arrows, chemical shift perturbation with phosphorylation. **B**, ^{15}N-^{13}C CON spectra of 100 μM ^{13}C,^{15}N δ1 tail alone (black) or in the presence of 100 μM CK1δΔC and 2.5 mM ATP for 2 hours at 25ºC (red). Arrows, chemical shift perturbation of the same peaks from panel B. **C**, Quantification of chemical shift perturbations ($\Delta\delta_{TOT}$, ppm) from the ^{15}N-^{13}C CON spectrum of the δ1 tail alone or after incubation with CK1δΔC and ATP. Dashed line, significance cutoff at 0.05 ppm; open circle, broadened peaks; *, unassigned peaks. **D**, Secondary Structure Propensity (SSP) analysis of the δ1 tail from chemical shift data. Random coil (blue), α-helix (pink), β-strand (black). **E**, Zoomed in view of CON spectra showing phosphorylation-dependent changes in the extreme C-terminus and predicted α-helical region. δ1 tail alone (black), with CK1δΔC and ATP for 2 hours at 25 ºC (red), or an unquenched partial phosphorylation reaction (orange). **F,** ^{15}N-^{1}H HSQC spectra of 34 μM δ1 tail alone (black) or in segmentally labeled kinase (gray). G296, only residue broadened in full-length kinase. **G**, ^{15}N-^{1}H HSQC spectra of ^{15}N δ1 tail with CK1δΔC and ATP in *trans* (red) or in *cis* (blue) with phosphopeak assignments. **H**, ^{15}N-edited 1D ^{1}H spectra of phosphopeaks in panel G. **I**, Quantification of 1D time course measuring phosphorylation of ^{15}N δ1 tail S406 in *trans* (red) or in *cis* (blue) with kinase. **J,** Representative western blot of purified CK1δ1 autophosphorylation detected with pSVV ab (n=3). **K,** Representative western blot of myc-CK1δ1 or myc-CK1δ1

S406/S407/S411A phosphorylation in cells treated with calyculin A (n=3). **L,** Representative western blot of CK1δ1 phosphorylation in cells treated with Cal A and PF 670 (n=3).

Fig 3

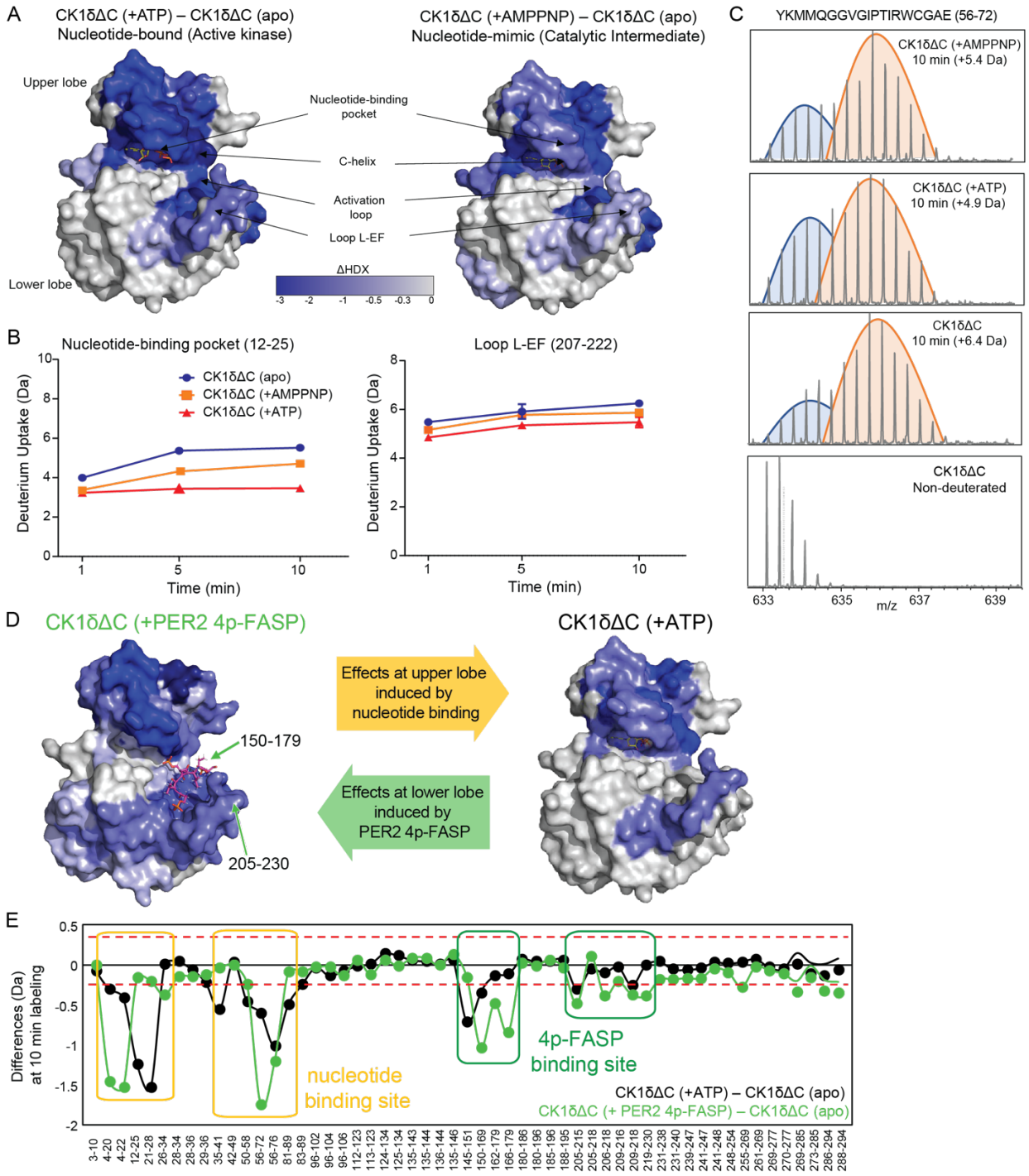
A
CK1δΔC (+ATP) – CK1δΔC (apo)
Nucleotide-bound (Active kinase)
CK1δΔC (+AMPPNP) – CK1δΔC (apo)
Nucleotide-mimic (Catalytic Intermediate)
Upper lobe
Lower lobe
Nucleotide-binding pocket
C-helix
Activation loop
Loop L-EF
ΔHDX
-3 -2 -1 -0.5 -0.3 0
B
Nucleotide-binding pocket (12-25)
Loop L-EF (207-222)
CK1δΔC (apo)
CK1δΔC (+AMPPNP)
CK1δΔC (+ATP)
Deuterium Uptake (Da)
Time (min)
C
YKMMQGGVGIPTIRWCGAE (56-72)
CK1δΔC (+AMPPNP) 10 min (+5.4 Da)
CK1δΔC (+ATP) 10 min (+4.9 Da)
CK1δΔC 10 min (+6.4 Da)
CK1δΔC Non-deuterated
m/z
D
CK1δΔC (+PER2 4p-FASP)
CK1δΔC (+ATP)
Effects at upper lobe induced by nucleotide binding
Effects at lower lobe induced by PER2 4p-FASP
150-179
205-230
E
Differences (Da) at 10 min labeling
nucleotide binding site
4p-FASP binding site
CK1δΔC (+ATP) – CK1δΔC (apo)
CK1δΔC (+ PER2 4p-FASP) – CK1δΔC (apo)

Figure 3 HDX-MS reveals dynamics in the CK1δ kinase domain in catalytic intermediate, active, and inhibited states

A, Structural representations of CK1δ kinase domain (PDB: 6PXO, with ATP (yellow) from PDB: 6RU6) indicating the regions with reduced deuterium exchange when saturated with ATP (left) or the ATP-analogue AMPPNP (right). Differences in deuterium exchange at 10 min labeling time are mapped in shades of blue as indicated. **B**, Kinetic plot of relative deuterium uptake for peptides spanning the nucleotide-binding pocket (left) and the catalytic loop (right) for CK1δΔC apo (blue), with ATP (red), or AMPPNP (orange). Average values (n = 6) from technical and biological replicates were used to generate the plot. **C**, Stacked mass spectral plots for peptide containing residues 56-72 with bimodal isotopic distribution at 10 min labeling time with lower (blue) and higher (orange) exchanging populations of CK1δΔC apo, or with ATP or AMPPNP, and a non-deuterated control. **D**, Structural representation of deuterium exchange at 10 min with ATP (right, PDB: 6PXO, with ATP (yellow) from PDB: 6RU6) or 4p-FASP (left, PDB: 8D7O). **E**, Comparison of differences in deuterium exchange of CK1δΔC in the presence and absence of 4p-FASP (green) or ATP (black) after 10 min labeling. Dashed line, significance threshold of ±0.28 Da. The deuterium exchange values are tabulated in Supplementary Table 1.

Fig 4

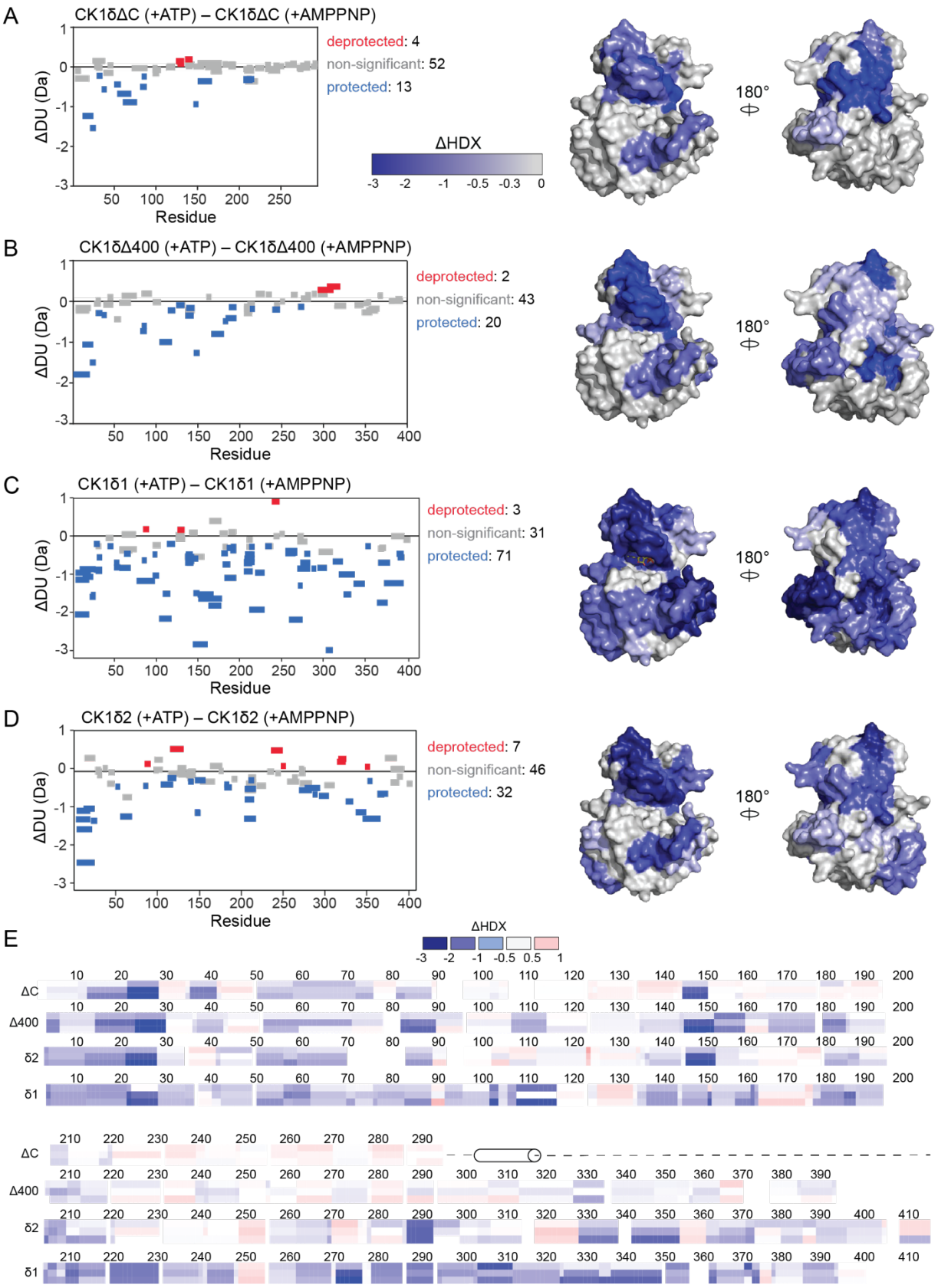
A
CK1δΔC (+ATP) – CK1δΔC (+AMPPNP)
deprotected: 4
non-significant: 52
protected: 13
ΔDU (Da)
Residue
ΔHDX
-3 -2 -1 -0.5 -0.3 0
180°
B
CK1δΔ400 (+ATP) – CK1δΔ400 (+AMPPNP)
deprotected: 2
non-significant: 43
protected: 20
C
CK1δ1 (+ATP) – CK1δ1 (+AMPPNP)
deprotected: 3
non-significant: 31
protected: 71
D
CK1δ2 (+ATP) – CK1δ2 (+AMPPNP)
deprotected: 7
non-significant: 46
protected: 32
E
ΔHDX
-3 -2 -1 -0.5 0.5 1
ΔC
Δ400
δ2
δ1

Figure 4 Impact of CK1δ tail on structural dynamics of the kinase.

A-D, Left, Woods differential plots showing deuterium exchange between ATP-bound and AMPPNP-bound states of different CK1δ constructs: (**A**) CK1δΔC; (**B**) CK1δΔ400; (**C**) CK1δ1; and (**D**) CK1δ2 at 10 min labeling time. Data available in Supplementary Table 2. Peptides showing significant protection (blue), deprotection (red), or non-significant (gray) deuterium exchange based on ±0.28 Da cutoff (confidence interval 99.0%). Right, corresponding structural representation of deuterium exchange differences at 10 min. **E**, Heat map of changes by residue in relative fractional uptake at 1 (top), 5 (middle), and 10 (bottom)-min labeling times for indicated constructs between ATP-bound and AMPPNP-bound states.

Fig 5

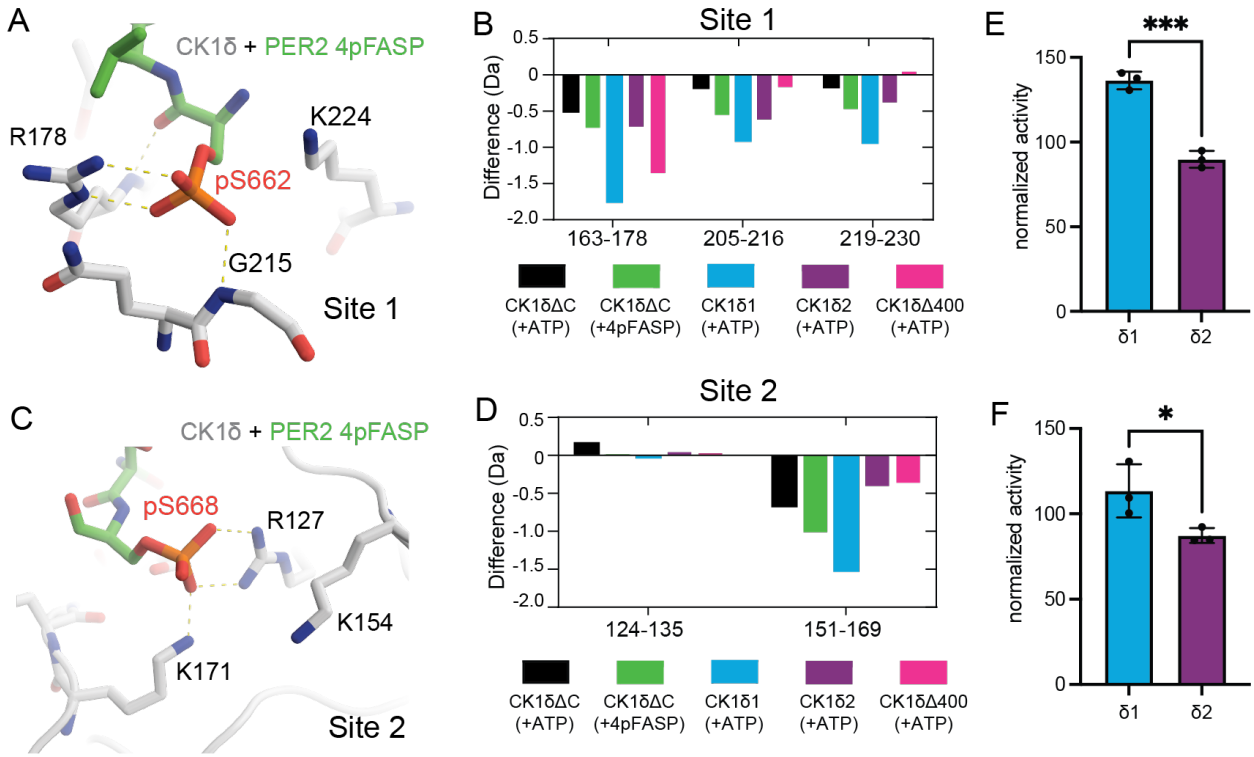

Figure 5 Anion binding sites on the kinase are required for autoinhibition by the δ1 tail

A, Structural view of CK1δ bound to the inhibitory PER2 4p-FASP (PDB: 8D70) showing phosphate coordination by anion binding site 1. **B**, Comparison of protection from deuterium exchange of peptides spanning anion binding site 1 with CK1δΔC (black), CK1δΔ400 (pink), CK1δ1 (blue), CK1δ2 (purple), and CK1δ-ΔC:4pFASP (green). **C**, Structural view of CK1δ bound to the inhibitory PER2 4p-FASP (PDB: 8D70) showing phosphate coordination by anion binding site 2. **D**, Comparison of protection from deuterium exchange of peptides spanning anion binding site 2. **E-F**, ^{32}P kinase assays comparing the activity of K224D (**E**) or R127E (**F**) in CK1δ1 (blue) and CK1δ2 (purple) to WT, normalized to the effect of the mutant on the isolated kinase domain (Fig. S5) (n=3, mean ± s.d.). Significance assessed by unpaired two-tailed t-test: *, $p<0.05$; ***, $p<0.001$.

Fig 6

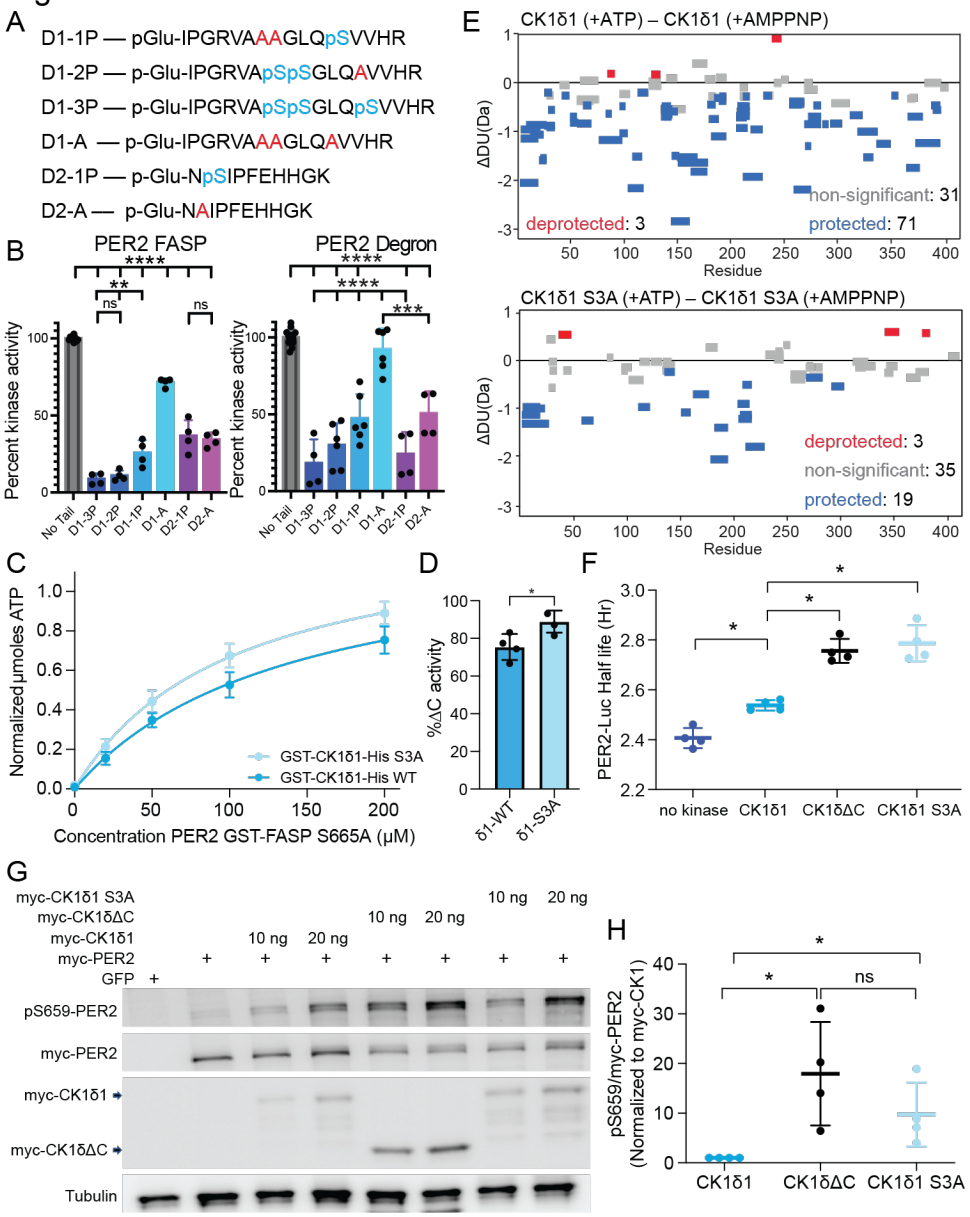
A
D1-1P — pGlu-IPGRVAAAGLQpSVVHR
D1-2P — p-Glu-IPGRVApSpSGLQAVVHR
D1-3P — p-Glu-IPGRVApSpSGLQpSVVHR
D1-A — p-Glu-IPGRVAAAGLQAVVHR
D2-1P — p-Glu-NpSIPFEHHGK
D2-A — p-Glu-NAIPFEHHGK
B
PER2 FASP
PER2 Degron
Percent kinase activity
No Tail
D1-3P
D1-2P
D1-1P
D1-A
D2-1P
D2-A
E
CK1δ1 (+ATP) – CK1δ1 (+AMPPNP)
ΔDU(Da)
Residue
deprotected: 3
non-significant: 31
protected: 71
CK1δ1 S3A (+ATP) – CK1δ1 S3A (+AMPPNP)
deprotected: 3
non-significant: 35
protected: 19
C
Normalized µmoles ATP
Concentration PER2 GST-FASP S665A (µM)
GST-CK1δ1-His S3A
GST-CK1δ1-His WT
D
%ΔC activity
δ1-WT
δ1-S3A
F
PER2-Luc Half life (Hr)
no kinase
CK1δ1
CK1δΔC
CK1δ1 S3A
G
myc-CK1δ1 S3A
myc-CK1δΔC
myc-CK1δ1
myc-PER2
GFP
10 ng
20 ng
pS659-PER2
myc-PER2
myc-CK1δ1
myc-CK1δΔC
Tubulin
H
pS659/myc-PER2 (Normalized to myc-CK1)
CK1δ1
CK1δΔC
CK1δ1 S3A
ns

Figure 6 Variable C-terminal tail length and mutations impacts kinase activity of CK1-δ on its substrate PER2.

A, Phosphorylated CK1δ C-terminal peptides; blue, phosphorylated serines (pS); red, alanine mutations to block phosphorylation. **B**, ADP-Glo kinase assay with phosphorylated CK1δ C-terminal peptides on PER2 FASP (left) or Degron (right). Significance assessed by ordinary one-way ANOVA **, $p<0.01$; ****, $p<0.0001$ (n=2, mean ± s.d.). **C**, ^{32}P kinase assay of CK1δ1 (blue) or the S3A mutant (light blue) on PER2 GST-FASP-S665A (n=3 mean ± s.d.). **D**, Quantification of panel C (n=3 mean + s.d.) Significance assessed by unpaired two-tailed t-test: *, $p<0.05$. **E**, Woods differential plots showing deuterium exchange between ATP-bound and AMPPNP-bound states of CK1δ1 (top) and CK1δ1 S3A (bottom) at 10 min labeling. Data available in Supplementary Table 2. Peptides showing significant protection (blue), deprotection (red) or non-significant (gray) deuterium exchange based on ±0.28 Da cutoff (confidence interval 99.0%). **F**, Half-life of PER2-Luc after co-transfection with 10 ng of indicated kinase constructs in HEK 293 cells (n=4 with mean ± s.d.). Significance assessed by unpaired two-tailed t-test: *, $p<0.05$. **G**, Representative western blot of mouse PER2 FASP priming phosphorylation (pS659) in HEK 293 lysates expressing indicated proteins (n=4). **H**, Quantification of PER2 FASP priming phosphorylation in panel G (n=4 with mean ± s.d.). Significance assessed by unpaired two-tailed t-test: *, $p<0.05$.

STAR Methods

RESOURCE AVAILABILITY

Lead contact

Further information and requests for resources and reagents should be directed to and will be fulfilled by the lead contact, Carrie L. Partch (cpartch@ucsc.edu).

Materials availability

- Plasmids generated in this study are available upon request.

Data availability

- Data generated in this study is included in the manuscript.
- NMR chemical shift assignments for the human CK1 δ1 and δ2 tails have been deposited at BMRB and will be publicly available upon publication.

EXPERIMENTAL MODEL AND SUBJECT DETAILS

Cell lines

- The HEK293T cell line was purchased from ATCC (#CRL-3216).

METHOD DETAILS

Protein constructs, expression, and purification

All constructs were expressed from TEV-cleavable vectors generated in-house based off the Parallel vector series (Sheffield et al., 1999) and have an N-terminal vector artifact (GAMDPEF) remaining after TEV cleavage. Mutations were introduced using the site-directed mutagenesis protocol in (Liu & Naismith, 2008) and validated by sequencing.

Full-length human CK1δ isoforms (CK1δ1, residues 1-415; CK1δ2, residues 1-409) and CK1δ Δ400 (residues 1-400) were expressed with an N-terminal TEV-cleavable

GST tag and a C-terminal His tag. Different constructs of the CK1δ catalytic domain, CK1δ ΔC (residues 1-294 or 1-317) were expressed with an N-terminal TEV-cleavable His-GST tag. A construct of the kinase domain for Sortase A-mediated ligations, CK1δ ΔC*, containing residues 1-294 with a C-terminal Sortase A recognition site (LPETGG) was expressed with an N-terminal TEV-cleavable His-MBP tag. Constructs of isolated CK1 tails (CK1δ1 tail, residues 295-415; CK1δ2 tail, residues 295-409; CK1δ1 short tail, residues 376-415) were expressed with an N-terminal TEV-cleavable His-NusA tag (HNXL) with an N-terminal tryptophan added for UV detection during purification.

Recombinantly expressed human PER2 peptides (FASP peptide, residues 645–687; Degron peptide, residues 475–505) were expressed with an N-terminal TEV-cleavable His-NusA tag when used for the ADP-Glo peptide inhibition assays or with an N-terminal TEV-cleavable His-GST tag for the radioactive kinase assay. All recombinant PER2 peptides contain an N-terminal tryptophan for UV detection during purification and a polybasic motif (WRKKK) following the vector artifact, as in (Philpott et al., 2022).

GST-lambda (λ) phosphatase-Strep-tag II was expressed with a TEV-cleavable N-terminal His-GST tag and a C-terminal Strep-tag II. His-Sortase A 7M (Addgene # 51141) and GST-λ phosphatase were expressed in BL21 (DE3) *Escherichia coli*, while all CK1 and PER constructs were expressed in Rosetta2 (DE3) *E. coli*. In general, cells were grown in LB media (for natural abundance growths) or M9 minimal media with the appropriate stable isotopes (i.e., $^{15}N/^{13}C$) for NMR as done before (Narasimamurthy et

al., 2018) at 37°C with shaking until the OD_{600} reached ~0.6-0.8. Expression was induced with 0.5 M IPTG, and cells were grown for an additional 16-20 hours at 18°C.

For purification of full-length CK1δ, cells were lysed in 50 mM Tris pH 7.5, 500 mM NaCl, 5% glycerol, 1 mM EDTA, 1 mM TCEP, 0.05% Tween using a high-pressure homogenizer. GST-tagged full-length proteins were purified from soluble lysate using Glutathione Sepharose resin (Cytiva) and eluted with buffer containing 50 mM Tris pH 7.5, 500 mM NaCl, 5% glycerol, 1 mM EDTA, 1 mM TCEP, 0.05% Tween, and 25 mM reduced glutathione. To remove phosphorylation from the kinase that may have occurred during expression or purification, GST-tagged purified proteins were treated with 200 nM GST-λ phosphatase-Strep tag II supplemented with 10 μM $MnCl_2$ in λ phosphatase buffer (50 mM HEPES pH 7.5, 100 mM NaCl, 0.1 mM EDTA, 1 mM TCEP) overnight at 4°C. Strep-Tactin Sepharose resin (Cytiva) was used to remove GST-λ phosphatase-Strep tag II, and dephosphorylated CK1δ was collected with several washes of 50 mM Tris pH 7.5, 500 mM NaCl, 5% glycerol, 1 mM EDTA, 1 mM TCEP, and 0.05% Tween. Dephosphorylated proteins were then further purified by the C-terminal His-tag using Ni-NTA resin (Qiagen). Full-length dephosphorylated proteins were subsequently purified by size-exclusion chromatography on a HiLoad 16/600 Superdex 200 prep grade column (Cytiva) in 50 mM Tris pH 7.5, 200 mM NaCl, 1 mM EDTA, 5 mM β-mercaptoethanol (BME), 5% glycerol, and 0.05% Tween, and then frozen in aliquots for storage at -70°C.

For CK1δ catalytic domain preps, cells were lysed in 50 mM Tris pH 7.5, 500 mM NaCl, 5% glycerol, 1 mM EDTA, 1 mM TCEP, 0.05% Tween using a high-pressure

homogenizer. His-GST-tagged proteins were purified from soluble lysate using Glutathione Sepharose resin (Cytiva) and eluted with 50 mM Tris pH 7.5, 500 mM NaCl, 5% glycerol, 1 mM EDTA, 1 mM TCEP, 0.05% Tween containing 25 mM reduced glutathione. To cleave the His-GST tag, His-TEV protease was incubated with the protein at 4°C overnight. Cleaved CK1δ ΔC was purified away from His-GST and His-TEV using Ni-NTA resin (Qiagen) and size-exclusion chromatography on a HiLoad 16/600 Superdex 75 prep grade column (Cytiva) in 25 mM MOPS pH 7.0, 1 mM EDTA, 100 mM NaCl, 5 mM BME, 11 mM $MgCl_2$, and 0.05% Tween, and then frozen in aliquots for storage at -70°C.

For CK1δ ΔC* preps, cells were lysed in 50 mM Tris pH 7.5, 500 mM NaCl, 2 mM TCEP, 5% glycerol and 25 mM imidazole using a high-pressure extruder homogenizer. His-MBP-CK1δ ΔC* was purified using Ni-NTA resin (Qiagen) using standard approaches and eluted from the resin using 50 mM Tris pH 7.5, 500 mM NaCl, 2 mM TCEP, 5% glycerol and 250 mM imidazole. His-TEV protease was added to cleave the His-MBP tag from the CK1δ ΔC* at 4°C overnight. The cleavage reaction was subsequently concentrated and diluted to low imidazole concentration (< 25 mM), and then the kinase was purified away from His-MBP and His-TEV using Ni-NTA resin with 50 mM Tris pH 7.5, 500 mM NaCl, 2 mM TCEP, 5% glycerol and 25 mM imidazole. Protein was collected from the flow-through, then further purified using ion exchange chromatography with a HiTrap SP XL column (Cytiva) preceding size-exclusion chromatography on a HiLoad 16/600 Superdex 75 prep grade column (Cytiva) in 25 mM MOPS pH 7.0, 1 mM EDTA, 100 mM NaCl, 5

mM BME, 11mM $MgCl_2$, and 0.05% Tween, and then frozen in aliquots for storage at -70°C.

For CK1δ1 tail and CK1δ2 tail preps, cells were lysed in 50 mM Tris pH 7.5, 500 mM NaCl, 2 mM TCEP, 5% glycerol and 25 mM imidazole using a high-pressure extruder homogenizer. His-NusA-tail fusion proteins were purified using Ni-NTA resin (Qiagen) using standard approaches and His-TEV protease was added to cleave the His-NusA tag from the tail on column at 4°C overnight. Tails were purified away from the resin containing His-NusA and His-TEV with 50 mM Tris pH 7.5, 500 mM NaCl, 2 mM TCEP, 5% glycerol and 25 mM imidazole. Tails were further purified by size exclusion chromatography on a HiLoad 16/600 Superdex 75 prep grade column (Cytiva) using NMR buffer (25 mM MOPS pH 7.0, 1 mM EDTA, 100 mM NaCl, 5 mM BME, 11 mM $MgCl_2$, and 0.05% Tween) and frozen in aliquots for storage at -70°C.

For PER2 peptide preps, cells were lysed in 50 mM Tris pH 7.5, 500 mM NaCl, 2 mM TCEP, 5% glycerol and 25 mM imidazole using a high-pressure extruder homogenizer. His-NusA-FASP or His-NusA-Degron fusion proteins were purified using Ni-NTA resin (Qiagen) using standard approaches and His-TEV protease was added to cleave the His-NusA tag from the PER2 peptides on column at 4°C overnight. Peptides were purified away from the resin containing His-NusA and His-TEV with 50 mM Tris pH 7.5, 500 mM NaCl, 2 mM TCEP, 5% glycerol and 25 mM imidazole. Peptides were purified by size exclusion chromatography on a HiLoad 16/600 Superdex 75 prep grade column (Cytiva) using 1X kinase buffer (25 mM Tris pH 7.5, 100 mM NaCl, 10 mM $MgCl_2$, and 2 mM

TCEP). For His-GST-tagged PER2 peptides used in the radioactive kinase assays, cells were lysed in 50 mM Tris pH 7.5, 500 mM NaCl, 5% glycerol, 1 mM EDTA, 1 mM TCEP, 0.05% Tween using a high-pressure homogenizer. His-GST-tagged proteins were purified from soluble lysate using Glutathione Sepharose resin (Cytiva) and eluted with 50 mM Tris pH 7.5, 500 mM NaCl, 5% glycerol, 1 mM EDTA, 1 mM TCEP, 0.05% Tween containing 25 mM reduced glutathione. The peptides were further purified using size-exclusion chromatography on a HiLoad 16/600 Superdex 75 prep grade column (Cytiva) in 25 mM Tris pH 7.5, 100 mM NaCl, 10 mM $MgCl_2$, and 2 mM TCEP, and then frozen in aliquots for storage at -70°C.

For His-Sortase A 7M, cells were lysed using a high-pressure extruder homogenizer followed by brief sonication at 4°C. After clarifying lysate on a centrifuge at 4°C at 140,500 × g for 1 hour, protein was captured using Ni-NTA affinity chromatography (Qiagen). The His-tag was cleaved using His-TEV protease on Ni-NTA resin at 4°C overnight. Cleaved protein was then collected from the flow-through and further purified using size exclusion chromatography on a HiLoad 16/600 Superdex 75 prep grade column (Cytiva) in 50 mM Tris, pH 7.5, 150 mM NaCl, and 10% glycerol, and then frozen in aliquots for storage at -70°C.

For GST-λ phosphatase-Strep tag II, cells were lysed in 50 mM Tris pH 7.5, 500 mM NaCl, 5% glycerol, 1 mM EDTA, 1 mM TCEP, 0.05% Tween using a high-pressure homogenizer. Proteins were purified from soluble lysate using Glutathione Sepharose resin (Cytiva) and eluted with a solution containing 50 mM Tris pH 7.5, 500 mM NaCl, 5%

glycerol, 1 mM EDTA, 1 mM TCEP, 0.05% Tween, and 25 mM reduced glutathione. λ-phosphatase was further purified using size-exclusion chromatography on a HiLoad 16/600 Superdex 75 prep grade column (Cytiva) in 50 mM HEPES pH 7.5, 100 mM NaCl, 0.1 mM EDTA, and 1 mM TCEP, and then frozen in aliquots for storage at -70°C.

Solid-phase synthesis of human PER2 and CK1δ peptides

The following peptides were synthesized via solid-phase methods and purified to >90% purity by Biopeptide, Co.: human PER2 4pFASP, GKAEpSVApSLTpSQCpSYA (where pS represents a phosphoserine); human CK1δ D1-1P, pGlu-IPGRVAAAGLQpSVVHR; human CK1δ D1-2P, pGlu-IPGRVApSpSGLQAVVHR; human CK1δ D1-3P, pGlu-IPGRVApSpSGLQpSVVHR; human CK1δ D1-A, pGlu-IPGRVAAAGLQAVVHR; human CK1δ D2-1P, pGlu-NpSIPFEHHGK; human CK1δ D2-A, pGlu-NAIPFEHHGK. Following peptides used for ELISA assay were synthesized by Genscript with ≥95% purity, human CK1-δ1 tail peptide: IPGRVASSGLQSVVHR, human CK1-δ1-3P-tail: IPGRVApSpSGLQpSVVHR.

Segmental labeling with Sortase A

To generate the segmentally isotopically labeled kinase, we utilized Sortase A-mediated ligation reactions (Theile et al., 2013) between a natural abundance kinase domain (CK1δ ΔC*, harboring the Sortase A recognition motif, LPETGG) and a uniformly ^{15}N-labeled CK1δ1 tail with a free N-terminal glycine left after TEV cleavage. The reaction was incubated and dialyzed overnight at 4°C in (50 mM Tris pH 7.5, 200 mM NaCl, 1 mM EDTA, 5 mM BME, and 0.05% Tween). The His-Sortase A 7M enzyme was purified away

from the reaction using Ni-NTA resin (Qiagen) with 50 mM Tris pH 7.5, 500 mM NaCl, 2 mM TCEP, 5% glycerol and 25 mM imidazole, while the ligated CK1δ ΔC*-^{15}N CK1δ1 tail product from the flow-through was further purified by size-exclusion chromatography on a Superdex 75 Increase 10/300 GL analytical grade column (Cytiva) in NMR buffer (25 mM MOPS pH 7.0, 1 mM EDTA, 100 mM NaCl, 5 mM BME, 11 mM $MgCl_2$, and 0.05% Tween) and frozen in aliquots for storage at -70°C.

***In vitro* kinase activity assays**

<u>ɣ^{32}P-ATP kinase assay</u>

Radioactive kinase assays were performed using human PER2 His-GST-FASP S665A or GST alone as the substrate. Reaction mixtures were prepared in reaction buffer (25 mM Tris pH 7.5, 200 mM NaCl, 10 mM $MgCl_2$, and 1 mM DTT) with 1 μM enzyme and 0-200 μM dilutions of the substrate as indicated at 25°C. Reactions were initiated with the addition of 2 mM ATP containing 2 μCi of ɣ-32p ATP (Perkin Elmer). All reactions were quenched with 2X SDS buffer after an incubation time of 1 hour. SDS-PAGE was performed on samples for each reaction, and the gels were dried at 80°C for 2 hours before being transferred to a storage phosphor screen (Amersham Biosciences) overnight. Images were collected with Typhoon Trio (Amersham Biosciences) and data were analyzed by densitometry using Image J (NIH), Excel (Microsoft), and Prism (GraphPad).

<u>ELISA-based kinase assay</u>

2 μg/mL of FASP-WT peptide was diluted in carbonate buffer, pH 9.5 and coated onto a 96 well plate (100 μL/well). The next day, 50 ng of CK1δ1-FL (from Signalchem) was incubated in kinase buffer (25 mM Tris pH 7.5, 5 mM beta glycerol phosphate, 2 mM DTT and 0.1 mM sodium orthovanadate) with or without 10 mM magnesium chloride and 200 μM ATP to allow for autophosphorylation for 30 min at 25°C in a reaction mixture of 20 μL. ELISA plate wells were washed thrice with wash buffer (PBS with 0.05% Tween 20, PBS-T) and once with kinase buffer. Reactions containing CK1δ1-FL purified protein with or without autophosphorylation were added to each well and the plate was incubated at 30°C for 1 hour. Next, the reaction mixture was discarded, and wells were washed with wash buffer thrice and incubated with blocking buffer (PBS-T with 5% BSA) for 1 hour at room temperature. Subsequently, wells were incubated with the polyclonal pS659 Ab, an anti-rabbit antibody conjugated to Biotin, and Streptavidin-HRP for 1 hour each at room temperature with washing as above after each incubation. For signal detection, TMB reagent (1-Step Ultra TMB-ELISA, Thermo Scientific) was added, incubated at room temperature for color development and quenched by addition of STOP solution (Thermo Scientific). The plate was read at 450 nm using an xMark Spectrophotometer plate reader (BioRad). Each sample was analyzed in triplicate.

ADP-Glo peptide inhibition assay

Kinase reactions were performed on the recombinant human PER2 FASP or Degron using the ADP-Glo kinase assay kit (Promega) according to manufacturer's instructions. Synthetic peptide inhibitors were solubilized in water at a concentration of 10 mM. All kinase reactions were performed in 30 μL reactions in duplicate (n = 3 independent

assays) with 100 μM ATP, 0.2 μM CK1δ ΔC kinase, and 50 μM FASP or 100 μM Degron substrates were incubated in 1X kinase buffer (25 mM Tris pH 7.5, 100 mM NaCl, 2 mM TCEP, 10 mM $MgCl_2$) at room temperature for 1 hour for FASP or 3 hours for Degron in the presence of increasing amounts of synthetic δ1 or δ2 peptides as indicated. 5 μL aliquots were quenched with ADP-Glo reagent after incubation, and luminescence measurements were taken at room temperature with a SYNERGY2 microplate reader (BioTek) in black opaque 384-well microplates. Data analysis was performed using Prism (GraphPad).

ELISA, Autophosphorylation, and Western Blotting

For ELISA, 1 μg/ml of indicated tail peptide was diluted in carbonate buffer, pH 9.5 and coated onto a 96 well ELISA plate (100 μl/well) and incubated overnight at 4. The next day, wells were washed with wash buffer (PBS with 0.05% Tween, PBS-T), blocked with blocking buffer for 1 hr (PBS-T with 5% BSA) and incubated with the pSVV antibody for 1 hr at room temperature (RT). Next, wells were incubated with anti-rabbit antibody conjugated to Biotin and further incubated with Streptavidin-HRP for detection. For signal detection, TMB (1-Step Ultra TMB-ELISA, Thermo Scientific) was added, incubated for color development and stopped by addition of STOP solution (Thermo Scientific), which was read at 450 nm using an xMark Spectrophotometer plate reader (BioRad). Each sample was analyzed in triplicate.

For autophosphorylation and subsequent analysis by Western blot, 75 ng of purified CK1δ1-FL protein (from Signalchem) was incubated in kinase buffer (25 mM Tris pH 7.5, 5 mM beta glycerol phosphate, 2 mM DTT and 0.1 mM sodium orthovanadate)

without or with 10 mM magnesium chloride and 200 μM ATP (for autophosphorylation) for 30 min at 25°C. Then, samples were added with Lammelli Buffer and processed according to the SDS-PAGE and Western blot protocol.

Either purified protein samples or whole cell extracts of transfected HEK293 cells lysed with cell lysis buffer (50 mM Tris-HCl pH 8.0, 150 mM NaCl, 1% Nonidet P-40, and 0.5% deoxycholic acid containing Complete protease inhibitors (Roche) and PhosStop phosphatase inhibitors (Roche)) were analyzed by denaturing SDS-PAGE gel, which was transferred on PVDF membrane (Immobilon, Millipore). Blot was further probed using indicated primary antibodies and appropriate secondary antibodies conjugated with HRP. Signal was detected with ECL reagents from Thermo Fisher Scientific. Densitometric analysis of WB bands were performed using the ImageJ software (National Institutes of Health).

PER2::LUC Half-life

Mouse PER2::LUC expression plasmids (10 ng) were transiently transfected alone or with myc-CK1δ1, myc-CK1δΔC, or myc-CK1δ1-S3A (10 ng) in 35 mm dishes of HEK293 cells in phenol red-free DMEM in the presence of 100 mM D-luciferin (#122799, PerkinElmer), 10 mM HEPES and 1.2 g/L sodium bicarbonate. Dishes were sealed with 40 mm cover glasses and vacuum grease and incubated in the LumiCycle (Actimetrics). The next day, 40 μg/mL cycloheximide (Sigma-Aldrich) was added per 35 mm dish. Luminescence data were used to calculate PER2::LUC half-life in Prism (GraphPad) using one-phase decay algorithm as described previously (Zhou et al., 2015). Briefly, half-lives were calculated using the one-phase decay algorithm in Prism (GraphPad) using the raw luciferase

activity, beginning from the point of cycloheximide addition to the plateau at minimum luciferase activity (n = 4).

NMR spectroscopy

NMR spectra were collected on a Varian INOVA 600 MHz, or a Bruker 800 MHz spectrometer equipped with a ^{1}H, ^{13}C, ^{15}N triple resonance z-axis pulsed-field-gradient cryoprobe. Spectra were processed using NMRPipe (Delaglio et al., 1995) and analyzed using CCPNmr Analysis (Vranken et al., 2005). Spectra were collected in NMR buffer (25 mM MOPS pH 7.0, 1 mM EDTA, 100 mM NaCl, 5 mM BME, 11 mM $MgCl_2$, and 0.05% Tween) with 10% D_2O at 25°C. The backbone assignment of the δ1 and δ2 tails was accomplished using standard NH-edited triple-resonance experiments [HN(CA)CO, HNCO, HNCACB, and CBCA(CO)NH] and four-dimensional carbon direct-detection methods such as (HACA)N(CA)CON and (HACA)N(CA)NCO. Phosphopeak assignments of the CK1δ1 short tail were accomplished using standard NH-edited triple-resonance experiments [HN(CA)CO, HNCO, and HNCACB].

Chemical shift perturbation (Δδ) or the change in ^{13}C-^{15}N CON peak position was calculated using the following equation:

$$\Delta\delta = \sqrt{(N\Delta_{ppm}\alpha)^2 + (CO\Delta_{ppm})^2}$$

where Δ_{ppm} is the change in chemical shift and a value of α = 0.3 was used to normalize between ^{15}N and ^{13}C chemical shift ranges. NMR kinase reactions were performed at 25°C with 100 μM ^{13}C,^{15}N CK1δ1 tail or CK1δ2 tail, 2.5 mM ATP and 100 μM CK1δ ΔC. Samples were incubated for 2 hours and quenched with 20 mM EDTA, then ^{1}H-^{15}N HSQC

spectra (total data acquisition = 20 min) and ^{13}C-^{15}N CON spectra (total acquisition time= 9 hr 32 min) were collected. The incubation time to reach saturation of the kinase reaction with CK1δ1 short tail was determined by collecting a series of ^{1}H-^{15}N HSQC spectra (53 20-min spectra for a total acquisition time = 1,060 min) of 100 μM ^{13}C,^{15}N CK1δ1 short tail, 2.5 mM ATP and 100 μM CK1δ ΔC at 25°C. For phosphopeak assignments, the CK1δ1 short tail kinase reaction was then performed with 100 μM ^{13}C,^{15}N CK1δ1 short tail, 2.5 mM ATP and 100 μM CK1δ ΔC incubated overnight at 25°C and quenched with 20 mM EDTA, then ^{1}H-^{15}N HSQC spectra (total data acquisition = 20 min), ^{13}C-^{15}N CON spectra (total acquisition time= 9 hr 32 min), and triple-resonance experiments were collected.

Segmentally labeled NMR kinase reactions were performed at 25°C with 34 μM CK1δ ΔC*-^{15}N CK1δ1 and 2.5 mM ATP. Samples were prepared as described above, and then ^{1}H-^{15}N HSQC spectra (total data acquisition= 2 hours) were collected. For the phosphorylation kinetic assays, reactions were performed at 25°C with 34 μM CK1δ ΔC*-^{15}N CK1δ1 tail, or 34 μM CK1δ ΔC* and 34 μM ^{15}N CK1δ1 tail in *trans*, and then ^{15}N-edited 1D ^{1}H spectra were collected (224 data points at 6 min per spectrum for a total data acquisition= 1,344 min) immediately after the addition of 2.5 mM ATP. Spectra were processed using MestreNova (MestreLab), and data analysis was performed using Excel (Microsoft) and Prism (GraphPad).

Hydrogen-deuterium exchange mass spectrometry

Sample preparation

To determine the effects of the nucleotide binding and monitor catalytic activity, hydrogen-deuterium exchange mass spectrometry (HDX-MS) was performed for different CK1δ constructs in the presence and absence of ATP or AMPPNP. Different CK1δ constructs were incubated with either ATP (~800 μM) or AMPPNP (~1.2 mM), or neither (apo), and 2 mM $MgCl_2$ for 15 min at 25 °C before each hydrogen-deuterium exchange reaction. For HDX of CK1δ ΔC bound to the PER2 4p-FASP peptide, an excess of the peptide substrate (2 mM final concentration) was incubated with CK1δ ΔC in the presence of ADP and $MgCl_2$. Hydrogen-deuterium labeling was initiated by diluting 60-65 pmol of CK1δ saturated with ATP or AMPPNP as indicated above in a reaction buffer prepared in deuterium oxide (D_2O, final concentration of 90%). Pulse-labeling reactions were carried out for 1, 5, and 10-minute timepoints, after which the exchange was minimized by lowering the pH to 2.5 and temperature to 0°C by adding pre-chilled quench solution (0.5 M Guanidinium hydrochloride, 0.1 M TCEP). Non-deuterated controls were carried out by diluting nucleotide-free CK1δ proteins in an aqueous reaction buffer instead of a deuterated buffer.

Mass spectrometry data acquisition

For nanoLC-MS/MS analyses, each quenched sample was subjected to in-line proteolysis using the Enzymate™ immobilized pepsin cartridge (Waters, USA). The digestion was left to proceed for 3 minutes at 12°C, and the resulting peptide mixtures were analyzed with nanoACQUITY M-class UPLC (Waters, UK) equipped with a trapping

column (VanGuard C18, 5 μm particle size) and an analytical column (BEH C18, 75 μm × 100 mm, 1.7 μm particle size) maintained at 3°C to minimize back-exchange (Wales et al., 2008). The aqueous solvent was 0.1% formic acid in LC-MS grade water, and the organic solvent was 0.1% formic acid in HPLC-grade acetonitrile. A 10-minute gradient was used to resolve and elute the peptides by reverse-phase chromatography. The peptides were then identified by Synapt G2-Si high-resolution mass spectrometer (Waters, UK). Briefly, the mass spectrometer was operated in positive polarity, data-independent (DIA) fragmentation and ion-mobility ($HDMS^E$) mode separation. Mass spectrometer parameters were as described previously (Raghuvamsi et al., 2021). Glu-fibrinopeptide reference (m/z = 785.8426) was continuously sprayed every 30 seconds during ESI-MS experiments using the lockspray device to ensure mass accuracy.

HDX data analysis

Peak lists for identifying and annotating the peptides from non-deuterated controls were generated by Protein Lynx Global Server v3.0 (Waters, USA), using human CK1δ (Uniprot: P48730) construct-specific protein database and searched against the parameters described previously (Raghuvamsi et al., 2021). Peptide mass measurements for individual peptides were assigned using DynamX v3.0 software (Waters, USA). Peptides with a minimum intensity of 2000, maximum length of 25 amino acids, and mass error within ± 10 ppm were considered for analysis. Deuterium exchange measurements were determined for all labeling timepoints across different protein states and were manually verified, but the data were not corrected for back-exchange. Only peptides with high signal-to-noise ratio and non-overlapping spectra were considered for final analysis. All measurements were done in biological duplicates and technical

triplicates, with statistical analysis done using Deuteros 2.0 (Lau et al., 2021) and tabulated as Supplementary Tables 1-3.

HDX data representation

Relative fractional deuterium uptake (RFU) is the ratio of the number of deuterons exchanged to the maximum number of available amides per peptide. Differences in deuterium exchange (ΔDU) were calculated as differences in centroid values of a deuterated peptide in protein condition with its corresponding deuterated peptide in a different protein condition. The pepsin digestion maps showing the sequence coverage of various CK1δ constructs and their corresponding deuterium uptake values are provided in Supplementary Tables 1 and 2. HDX profiles between different nucleotide bound CK1δ constructs indicated in Supplementary Figure S4 were compared by subtracting the RFU values for common peptides, as per the following scheme:

$\Delta DU = RFU_{CK1\delta1(+ATP)} - RFU_{x(+ATP)}$
where x = CK1δ2, CK1δ1 S3A, CK1δ Δ400, or CK1δ ΔC

QUANTIFICATION AND STATISTICAL ANALYSIS

All statistical analyses were done using Prism (GraphPad). P-values were calculated using Students t-test, one-way ANOVA with Tukey's multiple comparisons test, or extra sum of squares F-test as indicated in different figures. In all figures, * indicates $p<0.05$, **$p<0.01$, ***$p<0.001$, ****$p<0.0001$, ns, not significant.

Supplementary Material

Supplementary Table 1

Deuterium exchange values for various pepsin-digested peptides of CK1δΔC in the presence of ATP, AMPPNP, and 4p-FASP at 1, 5, and 10-minute labeling times are tabulated.

Supplementary Table 2

Deuterium exchange values for various pepsin-digested peptides of CK1δ1, CK1δ2, CK1δ1 S3A, and CK1δ1ΔC in the presence of ATP, AMPPNP, and 4p-FASP at 1, 5, and 10-minute labeling times are tabulated.

Supplementary Table 3

HDX metadata table depicting the experimental conditions for different CK1δ1 isoforms, and the corresponding analysis is represented.

References

An, Y., Yuan, B., Xie, P., Gu, Y., Liu, Z., Wang, T., Li, Z., Xu, Y., & Liu, Y. (2022). Decoupling PER phosphorylation, stability and rhythmic expression from circadian clock function by abolishing PER-CK1 interaction. *Nat Commun*, *13*(1), 3991. https://doi.org/10.1038/s41467-022-31715-4

Arbesu, M., Iruela, G., Fuentes, H., Teixeira, J. M. C., & Pons, M. (2018). Intramolecular Fuzzy Interactions Involving Intrinsically Disordered Domains. *Front Mol Biosci*, *5*, 39. https://doi.org/10.3389/fmolb.2018.00039

Aryal, R. P., Kwak, P. B., Tamayo, A. G., Gebert, M., Chiu, P. L., Walz, T., & Weitz, C. J. (2017). Macromolecular Assemblies of the Mammalian Circadian Clock. *Mol Cell*, *67*(5), 770-782 e776. https://doi.org/10.1016/j.molcel.2017.07.017

Bastidas, M., Gibbs, E. B., Sahu, D., & Showalter, S. A. (2015). A primer for carbon-detected NMR applications to intrinsically disordered proteins in solution. *Concepts in Magnetic Resonance Part A*, *44*(1), 54-66. https://doi.org/https://doi.org/10.1002/cmr.a.21327

Bischof, J., Randoll, S. J., Sussner, N., Henne-Bruns, D., Pinna, L. A., & Knippschild, U. (2013). CK1delta kinase activity is modulated by Chk1-mediated phosphorylation. *PLoS One*, *8*(7), e68803. https://doi.org/10.1371/journal.pone.0068803

Brockschmidt, C., Hirner, H., Huber, N., Eismann, T., Hillenbrand, A., Giamas, G., Radunsky, B., Ammerpohl, O., Bohm, B., Henne-Bruns, D., Kalthoff, H., Leithauser, F., Trauzold, A., & Knippschild, U. (2008). Anti-apoptotic and growth-stimulatory functions of CK1 delta and epsilon in ductal adenocarcinoma of the pancreas are inhibited by IC261 in vitro and in vivo. *Gut*, *57*(6), 799-806. https://doi.org/10.1136/gut.2007.123695

Cao, X., Wang, L., Selby, C. P., Lindsey-Boltz, L. A., & Sancar, A. (2023). Analysis of Mammalian Circadian Clock Protein Complexes Over a Circadian Cycle. *J Biol Chem*, 102929. https://doi.org/10.1016/j.jbc.2023.102929

Cao, X., Yang, Y., Selby, C. P., Liu, Z., & Sancar, A. (2021). Molecular mechanism of the repressive phase of the mammalian circadian clock. *Proc Natl Acad Sci U S A*, *118*(2). https://doi.org/10.1073/pnas.2021174118

Cegielska, A., Gietzen, K. F., Rivers, A., & Virshup, D. M. (1998). Autoinhibition of casein kinase I epsilon (CKI epsilon) is relieved by protein phosphatases and limited proteolysis. *J Biol Chem*, *273*(3), 1357-1364. https://doi.org/10.1074/jbc.273.3.1357

Cruciat, C. M. (2014). Casein kinase 1 and Wnt/beta-catenin signaling. *Curr Opin Cell Biol*, *31*, 46-55. https://doi.org/10.1016/j.ceb.2014.08.003

Cullati, S. N., Chaikuad, A., Chen, J. S., Gebel, J., Tesmer, L., Zhubi, R., Navarrete-Perea, J., Guillen, R. X., Gygi, S. P., Hummer, G., Dotsch, V., Knapp, S., & Gould, K. L. (2022). Kinase domain autophosphorylation rewires the activity and substrate specificity of CK1 enzymes. *Mol Cell*, *82*(11), 2006-2020 e2008. https://doi.org/10.1016/j.molcel.2022.03.005

Dahlberg, C. L., Nguyen, E. Z., Goodlett, D., & Kimelman, D. (2009). Interactions between Casein kinase Iepsilon (CKIepsilon) and two substrates from disparate signaling pathways reveal mechanisms for substrate-kinase specificity. *PLoS One*, *4*(3), e4766. https://doi.org/10.1371/journal.pone.0004766

Del Valle-Perez, B., Arques, O., Vinyoles, M., de Herreros, A. G., & Dunach, M. (2011). Coordinated action of CK1 isoforms in canonical Wnt signaling. *Mol Cell Biol*, *31*(14), 2877-2888. https://doi.org/10.1128/MCB.01466-10

Delaglio, F., Grzesiek, S., Vuister, G. W., Zhu, G., Pfeifer, J., & Bax, A. (1995). NMRPipe: a multidimensional spectral processing system based on UNIX pipes. *J Biomol NMR*, *6*(3), 277-293. https://doi.org/10.1007/BF00197809

Dyla, M., & Kjaergaard, M. (2020). Intrinsically disordered linkers control tethered kinases via effective concentration. *Proc Natl Acad Sci U S A*, *117*(35), 21413-21419. https://doi.org/10.1073/pnas.2006382117

Endicott, J. A., Noble, M. E., & Johnson, L. N. (2012). The structural basis for control of eukaryotic protein kinases. *Annu Rev Biochem*, *81*, 587-613. https://doi.org/10.1146/annurev-biochem-052410-090317

Eng, G. W. L., Edison, & Virshup, D. M. (2017). Site-specific phosphorylation of casein kinase 1 delta (CK1delta) regulates its activity towards the circadian regulator

PER2. *PLoS One*, *12*(5), e0177834. https://doi.org/10.1371/journal.pone.0177834
Etchegaray, J. P., Machida, K. K., Noton, E., Constance, C. M., Dallmann, R., Di Napoli, M. N., DeBruyne, J. P., Lambert, C. M., Yu, E. A., Reppert, S. M., & Weaver, D. R. (2009). Casein kinase 1 delta regulates the pace of the mammalian circadian clock. *Mol Cell Biol*, *29*(14), 3853-3866. https://doi.org/10.1128/MCB.00338-09
Fustin, J. M., Kojima, R., Itoh, K., Chang, H. Y., Ye, S., Zhuang, B., Oji, A., Gibo, S., Narasimamurthy, R., Virshup, D., Kurosawa, G., Doi, M., Manabe, I., Ishihama, Y., Ikawa, M., & Okamura, H. (2018). Two Ck1delta transcripts regulated by m6A methylation code for two antagonistic kinases in the control of the circadian clock. *Proc Natl Acad Sci U S A*, *115*(23), 5980-5985. https://doi.org/10.1073/pnas.1721371115
Gao, Z. H., Seeling, J. M., Hill, V., Yochum, A., & Virshup, D. M. (2002). Casein kinase I phosphorylates and destabilizes the beta-catenin degradation complex. *Proc Natl Acad Sci U S A*, *99*(3), 1182-1187. https://doi.org/10.1073/pnas.032468199
Gebel, J., Tuppi, M., Chaikuad, A., Hotte, K., Schroder, M., Schulz, L., Lohr, F., Gutfreund, N., Finke, F., Henrich, E., Mezhyrova, J., Lehnert, R., Pampaloni, F., Hummer, G., Stelzer, E. H. K., Knapp, S., & Dotsch, V. (2020). p63 uses a switch-like mechanism to set the threshold for induction of apoptosis. *Nat Chem Biol*, *16*(10), 1078-1086. https://doi.org/10.1038/s41589-020-0600-3
Giamas, G., Hirner, H., Shoshiashvili, L., Grothey, A., Gessert, S., Kuhl, M., Henne-Bruns, D., Vorgias, C. E., & Knippschild, U. (2007). Phosphorylation of CK1delta: identification of Ser370 as the major phosphorylation site targeted by PKA in vitro and in vivo. *Biochem J*, *406*(3), 389-398. https://doi.org/10.1042/BJ20070091
Graves, P. R., & Roach, P. J. (1995). Role of COOH-terminal phosphorylation in the regulation of casein kinase I delta. *J Biol Chem*, *270*(37), 21689-21694. https://doi.org/10.1074/jbc.270.37.21689
Hamuro, Y., Wong, L., Shaffer, J., Kim, J. S., Stranz, D. D., Jennings, P. A., Woods, V. L., Jr., & Adams, J. A. (2002). Phosphorylation driven motions in the COOH-terminal Src kinase, CSK, revealed through enhanced hydrogen-deuterium exchange and mass spectrometry (DXMS). *J Mol Biol*, *323*(5), 871-881. https://doi.org/10.1016/s0022-2836(02)01003-3
Hubbard, S. R. (1997). Crystal structure of the activated insulin receptor tyrosine kinase in complex with peptide substrate and ATP analog. *EMBO J*, *16*(18), 5572-5581. https://doi.org/10.1093/emboj/16.18.5572
Huse, M., & Kuriyan, J. (2002). The conformational plasticity of protein kinases. *Cell*, *109*(3), 275-282. https://doi.org/10.1016/s0092-8674(02)00741-9
Knippschild, U., Kruger, M., Richter, J., Xu, P., Garcia-Reyes, B., Peifer, C., Halekotte, J., Bakulev, V., & Bischof, J. (2014). The CK1 Family: Contribution to Cellular Stress Response and Its Role in Carcinogenesis. *Front Oncol*, *4*, 96. https://doi.org/10.3389/fonc.2014.00096
Knippschild, U., Wolff, S., Giamas, G., Brockschmidt, C., Wittau, M., Wurl, P. U., Eismann, T., & Stoter, M. (2005). The role of the casein kinase 1 (CK1) family in different signaling pathways linked to cancer development. *Onkologie*, *28*(10), 508-514. https://doi.org/10.1159/000087137

Kobashigawa, Y., Kumeta, H., Ogura, K., & Inagaki, F. (2009). Attachment of an NMR-invisible solubility enhancement tag using a sortase-mediated protein ligation method. *J Biomol NMR*, *43*(3), 145-150. https://doi.org/10.1007/s10858-008-9296-5

Konermann, L., Pan, J., & Liu, Y. H. (2011). Hydrogen exchange mass spectrometry for studying protein structure and dynamics. *Chem Soc Rev*, *40*(3), 1224-1234. https://doi.org/10.1039/c0cs00113a

Lau, A. M., Claesen, J., Hansen, K., & Politis, A. (2021). Deuteros 2.0: peptide-level significance testing of data from hydrogen deuterium exchange mass spectrometry. *Bioinformatics*, *37*(2), 270-272. https://doi.org/10.1093/bioinformatics/btaa677

Lee, H., Chen, R., Lee, Y., Yoo, S., & Lee, C. (2009). Essential roles of CKIdelta and CKIepsilon in the mammalian circadian clock. *Proc Natl Acad Sci U S A*, *106*(50), 21359-21364. https://doi.org/10.1073/pnas.0906651106

Lee, T., Hoofnagle, A. N., Resing, K. A., & Ahn, N. G. (2005). Hydrogen exchange solvent protection by an ATP analogue reveals conformational changes in ERK2 upon activation. *J Mol Biol*, *353*(3), 600-612. https://doi.org/10.1016/j.jmb.2005.08.029

Liu, F., Virshup, D. M., Nairn, A. C., & Greengard, P. (2002). Mechanism of regulation of casein kinase I activity by group I metabotropic glutamate receptors. *J Biol Chem*, *277*(47), 45393-45399. https://doi.org/10.1074/jbc.M204499200

Liu, H., & Naismith, J. H. (2008). An efficient one-step site-directed deletion, insertion, single and multiple-site plasmid mutagenesis protocol. *BMC Biotechnol*, *8*, 91. https://doi.org/10.1186/1472-6750-8-91

Longenecker, K. L., Roach, P. J., & Hurley, T. D. (1998). Crystallographic studies of casein kinase I delta toward a structural understanding of auto-inhibition. *Acta Crystallogr D Biol Crystallogr*, *54*(Pt 3), 473-475. https://doi.org/10.1107/s0907444997011724

Lorenzen, K., & Pawson, T. (2014). HDX-MS takes centre stage at unravelling kinase dynamics. *Biochem Soc Trans*, *42*(1), 145-150. https://doi.org/10.1042/BST20130250

Lowrey, P. L., Shimomura, K., Antoch, M. P., Yamazaki, S., Zemenides, P. D., Ralph, M. R., Menaker, M., & Takahashi, J. S. (2000). Positional syntenic cloning and functional characterization of the mammalian circadian mutation tau. *Science*, *288*(5465), 483-492. https://doi.org/10.1126/science.288.5465.483

Masson, G. R., Burke, J. E., Ahn, N. G., Anand, G. S., Borchers, C., Brier, S., Bou-Assaf, G. M., Engen, J. R., Englander, S. W., Faber, J., Garlish, R., Griffin, P. R., Gross, M. L., Guttman, M., Hamuro, Y., Heck, A. J. R., Houde, D., Iacob, R. E., Jorgensen, T. J. D., . . . Rand, K. D. (2019). Recommendations for performing, interpreting and reporting hydrogen deuterium exchange mass spectrometry (HDX-MS) experiments. *Nat Methods*, *16*(7), 595-602. https://doi.org/10.1038/s41592-019-0459-y

Narasimamurthy, R., Hunt, S. R., Lu, Y., Fustin, J. M., Okamura, H., Partch, C. L., Forger, D. B., Kim, J. K., & Virshup, D. M. (2018). CK1delta/epsilon protein kinase primes the PER2 circadian phosphoswitch. *Proc Natl Acad Sci U S A*, *115*(23), 5986-5991. https://doi.org/10.1073/pnas.1721076115

Narasimamurthy, R., & Virshup, D. M. (2021). The phosphorylation switch that regulates ticking of the circadian clock. *Mol Cell*, *81*(6), 1133-1146. https://doi.org/10.1016/j.molcel.2021.01.006

Oppermann, F. S., Gnad, F., Olsen, J. V., Hornberger, R., Greff, Z., Keri, G., Mann, M., & Daub, H. (2009). Large-scale proteomics analysis of the human kinome. *Mol Cell Proteomics*, *8*(7), 1751-1764. https://doi.org/10.1074/mcp.M800588-MCP200

Partch, C. L., Shields, K. F., Thompson, C. L., Selby, C. P., & Sancar, A. (2006). Posttranslational regulation of the mammalian circadian clock by cryptochrome and protein phosphatase 5. *Proc Natl Acad Sci U S A*, *103*(27), 10467-10472. https://doi.org/10.1073/pnas.0604138103

Philpott, J. M., Freeberg, A. M., Park, J., Lee, K., Ricci, C. G., Hunt, S. R., Narasimamurthy, R., Segal, D. H., Robles, R., Cai, Y. D., Tripathi, S., McCammon, J. A., Virshup, D. M., Chiu, J. C., Lee, C., & Partch, C. L. (2022). PERIOD phosphorylation leads to feedback inhibition of CK1 activity to control circadian period. *bioRxiv*, 2022.2006.2024.497549. https://doi.org/10.1101/2022.06.24.497549

Philpott, J. M., Narasimamurthy, R., Ricci, C. G., Freeberg, A. M., Hunt, S. R., Yee, L. E., Pelofsky, R. S., Tripathi, S., Virshup, D. M., & Partch, C. L. (2020). Casein kinase 1 dynamics underlie substrate selectivity and the PER2 circadian phosphoswitch. *Elife*, *9*. https://doi.org/10.7554/eLife.52343

Raghuvamsi, P. V., Tulsian, N. K., Samsudin, F., Qian, X., Purushotorman, K., Yue, G., Kozma, M. M., Hwa, W. Y., Lescar, J., Bond, P. J., MacAry, P. A., & Anand, G. S. (2021). SARS-CoV-2 S protein:ACE2 interaction reveals novel allosteric targets. *Elife*, *10*. https://doi.org/10.7554/eLife.63646

Ralph, M. R., & Menaker, M. (1988). A mutation of the circadian system in golden hamsters. *Science*, *241*(4870), 1225-1227. https://doi.org/10.1126/science.3413487

Rivers, A., Gietzen, K. F., Vielhaber, E., & Virshup, D. M. (1998). Regulation of casein kinase I epsilon and casein kinase I delta by an in vivo futile phosphorylation cycle. *J Biol Chem*, *273*(26), 15980-15984. https://doi.org/10.1074/jbc.273.26.15980

Rosenberg, L. H., Lafitte, M., Quereda, V., Grant, W., Chen, W., Bibian, M., Noguchi, Y., Fallahi, M., Yang, C., Chang, J. C., Roush, W. R., Cleveland, J. L., & Duckett, D. R. (2015). Therapeutic targeting of casein kinase 1delta in breast cancer. *Sci Transl Med*, *7*(318), 318ra202. https://doi.org/10.1126/scitranslmed.aac8773

Sacco, F., Humphrey, S. J., Cox, J., Mischnik, M., Schulte, A., Klabunde, T., Schafer, M., & Mann, M. (2016). Glucose-regulated and drug-perturbed phosphoproteome reveals molecular mechanisms controlling insulin secretion. *Nat Commun*, *7*, 13250. https://doi.org/10.1038/ncomms13250

Schittek, B., & Sinnberg, T. (2014). Biological functions of casein kinase 1 isoforms and putative roles in tumorigenesis. *Mol Cancer*, *13*, 231. https://doi.org/10.1186/1476-4598-13-231

Sheetz, J. B., Lemmon, M. A., & Tsutsui, Y. (2022). Dynamics of protein kinases and pseudokinases by HDX-MS. *Methods Enzymol*, *667*, 303-338. https://doi.org/10.1016/bs.mie.2022.03.037

Sheffield, P., Garrard, S., & Derewenda, Z. (1999). Overcoming expression and purification problems of RhoGDI using a family of "parallel" expression vectors. *Protein Expr Purif*, *15*(1), 34-39. https://doi.org/10.1006/prep.1998.1003

Shi, Z., Resing, K. A., & Ahn, N. G. (2006). Networks for the allosteric control of protein kinases. *Curr Opin Struct Biol*, *16*(6), 686-692. https://doi.org/10.1016/j.sbi.2006.10.011

Theile, C. S., Witte, M. D., Blom, A. E., Kundrat, L., Ploegh, H. L., & Guimaraes, C. P. (2013). Site-specific N-terminal labeling of proteins using sortase-mediated reactions. *Nat Protoc*, *8*(9), 1800-1807. https://doi.org/10.1038/nprot.2013.102

Toh, K. L., Jones, C. R., He, Y., Eide, E. J., Hinz, W. A., Virshup, D. M., Ptacek, L. J., & Fu, Y. H. (2001). An hPer2 phosphorylation site mutation in familial advanced sleep phase syndrome. *Science*, *291*(5506), 1040-1043. https://doi.org/10.1126/science.1057499

Um, J. H., Yang, S., Yamazaki, S., Kang, H., Viollet, B., Foretz, M., & Chung, J. H. (2007). Activation of 5'-AMP-activated kinase with diabetes drug metformin induces casein kinase Iepsilon (CKIepsilon)-dependent degradation of clock protein mPer2. *J Biol Chem*, *282*(29), 20794-20798. https://doi.org/10.1074/jbc.C700070200

Vranken, W. F., Boucher, W., Stevens, T. J., Fogh, R. H., Pajon, A., Llinas, M., Ulrich, E. L., Markley, J. L., Ionides, J., & Laue, E. D. (2005). The CCPN data model for NMR spectroscopy: development of a software pipeline. *Proteins*, *59*(4), 687-696. https://doi.org/10.1002/prot.20449

Wales, T. E., Fadgen, K. E., Gerhardt, G. C., & Engen, J. R. (2008). High-speed and high-resolution UPLC separation at zero degrees Celsius. *Anal Chem*, *80*(17), 6815-6820. https://doi.org/10.1021/ac8008862

Wang, W., & Wang, D. (2019). Extreme Fuzziness: Direct Interactions between Two IDPs. *Biomolecules*, *9*(3). https://doi.org/10.3390/biom9030081

Xu, Y., Padiath, Q. S., Shapiro, R. E., Jones, C. R., Wu, S. C., Saigoh, N., Saigoh, K., Ptacek, L. J., & Fu, Y. H. (2005). Functional consequences of a CKIdelta mutation causing familial advanced sleep phase syndrome. *Nature*, *434*(7033), 640-644. https://doi.org/10.1038/nature03453

Xu, Y., Toh, K. L., Jones, C. R., Shin, J. Y., Fu, Y. H., & Ptacek, L. J. (2007). Modeling of a human circadian mutation yields insights into clock regulation by PER2. *Cell*, *128*(1), 59-70. https://doi.org/10.1016/j.cell.2006.11.043

Zhou, M., Kim, J. K., Eng, G. W., Forger, D. B., & Virshup, D. M. (2015). A Period2 Phosphoswitch Regulates and Temperature Compensates Circadian Period. *Mol Cell*, *60*(1), 77-88. https://doi.org/10.1016/j.molcel.2015.08.022